4.09 Material Performance in Molten Salt[☆]

Yoonjo (Jo Jo) Lee, Materials Science and Technology Division, Oak Ridge National Laboratory, Oak Ridge, TN, United States

Nomenclature

$^{1}_{0}n$ Notation representing neutron in a nuclear reaction
$^{3}_{1}H$ Notation for tritium in a nuclear reaction
$^{3}_{1}HF$ Notation for tritium fluoride in a nuclear reaction
$^{4}_{2}\alpha$ Notation representing alpha particle (helium nucleus) in a nuclear reaction
$^{6}_{2}He$ Notation for transmutated helium in a nuclear reaction
e^{+} Notation for beta particle with positive charge (positron) emitted in a nuclear reaction
γ_e Notation for neutrino, massless particle
^{135}Xe Radioisotope of Xe, a neutron poison
^{232}Th Naturally occurring radionuclide of Th (fertile)
^{233}Pa Radioisotope of Pa, neutron poison
^{233}U Fissile isotope of U
^{235}U Naturally occurring (~0.72%) radionuclide of U (fissile)
^{238}U Naturally occurring (~99.3%) radionuclide of U (fertile)
^{239}Pu Non naturally-occurring radionuclide from transmutation of ^{238}U (fissile)
316H A 316 stainless steel, H indicates high carbon formulation
^{35}Cl Naturally-occurring (~76%) stable isotope of Cl
^{36}Cl Radionuclide of Cl from neutron activation of ^{35}Cl
^{37}Cl Naturally-occurring (~24.2%) stable isotope of Cl
^{6}Li Naturally occurring (~92.5%) radionuclide of Li
^{7}Li Naturally occurring (~7.5%) radionuclide of Li
barns SI unit of nuclear reaction cross-sections equivalent to 10^{-24} cm^2
BeF_2 Beryllium fluoride
BeO Beryllium oxide
BF_4 Fluoroborate
$CeCl_3$ Cerium chloride
CeF_3 Cerium trifluoride (PuF_3 surrogate)
CsI Cesium iodide
FLiBe Eutectic binary LiF–BeF_2 salt mixture
FLiNaK Eutectic ternary LiF–NaF–KF salt mixture
GH3535 Ni-base alloy developed by Chinese Academy of Sciences
HEU High-enriched U (>20% ^{235}U)
KF Potassium fluoride
LEU Low-enriched U (<20% ^{235}U)
LiF Lithium fluoride
NaF Sodium fluoride
Pa_2O_5 Protactinium oxide
PaF_2 Protactinium fluoride
$PuCl_3$ Plutonium trichloride
PuF_3 Plutonium trifluoride
PuF_4 Plutonium tetrafluoride
SCRAM Terminology for emergency shut down of a nuclear reactor

[☆]*Change History*: October 2019. Yoonjo (Jo Jo) Lee has updated the text and references.
This is an update of Ignatiev, V., Surenkov, A., 2012. Chapter 5.10 – Material Performance in Molten Salts. In: Konings, R.J.M. (Ed.), Comprehensive Nuclear Materials, Elsevier, pp. 221–250.

 doi:10.1016/B978-0-12-803581-8.00750-5

ThF_4 Thorium tetrafluoride
UCl_3 Uranium trichloride
UF_3 Uranium trifluoride
UF_4 Uranium tetrafluoride
UF_4 Uranium tetrafluoride
ZrF_4 Zirconium tetrafluoride
σ_{th} Thermal neutron capture cross-section

4.09.1 Introduction: History, Scope, and Application

Molten salt is a liquid obtained from fusion of an inorganic salt – fluorides, carbonates, nitrates, etc. They are an important class of engineering fluids for high temperature energy storage and heat transfer applications. For advanced nuclear systems, molten salts are applicable as coolants and fuel solvents in fission and breeder reactors and have been considered for the blanket of fusion reactors. Melting points of salts are fairly indicative of the lower temperature limit and the type of application. Salt compositions can be further fine-tuned to the application by using mixtures or additives. Some common advantages of molten salts are (1) high temperature stability, (2) low vapor pressure, (3) liquid state in a large temperature range, and (4) high solubility for many inorganic and organic compounds.[1] Prior to the early nuclear applications of fluoride salts by Oak Ridge National Laboratory (ORNL) in the 1950s, there was experience with nitrate molten salts for heat transfer and thermal energy storage in the chemical industry. Today, Li, Na, and K nitrate salts and relevant mixtures along with chloride salts are still important molten salts for concentrated solar power technologies.[2]

When considering materials performance in molten salt reactors (MSR), corrosion and radiation damage are typically the main degradation mechanisms that shorten the service life of materials. Advanced next generation high temperature reactors supply process heat between 700 and 950°C for electric power generation and hydrogen production for a future hydrogen economy. At these temperatures, the problems with metals are apparent, and metals cannot be used in the high flux regions of the core. Thus, it has been argued by some that developing ceramic composites and coatings is one of the promising paths forward.[3] This article mainly focuses on materials corrosion or compatibility in molten salt. Radiation effects are also discussed but some topics have been simplified to enhance understanding of overall material performance and lifetime assessments for components.

4.09.1.1 Molten Salt Reactor Experiment History

The use of molten salt as a coolant and solvent for nuclear fuel in fission and breeder reactor concepts dates back to 1947. Upon the initiative and recommendations of several colleagues, Ed Bettis and Ray Briant at ORNL proposed a molten salt-cooled nuclear reactor for a nuclear-powered aircraft, known as the Aircraft Reactor Experiment (ARE).[4,5] The first two uses of molten fluoride salts for nuclear applications occurred at ORNL during 1954 for 1000 h with ARE and from 1965 to 1969 with the Molten Salt Reactor Experiment (MSRE). The ARE was the first MSR using a circulating liquid fuel of fused fluoride salt mixture of NaF, ZrF_4 and UF_4, producing around 2.5 MW_{th}, and the moderator was blocks of BeO.[4] Subsequently, a longer demonstration was needed to test the viability of a liquid fueled nuclear reactor, which became MSRE. MSRE had an unclad graphite-moderated core, was constructed from Ni-base alloy INOR-8 (later known commercially as Hastelloy N) and used LiF–BeF_2–ZrF_4–UF_4 (65–29.1–5–0.9 mol%) fuel salt. The core consisted of a lattice of about 600 graphite bars, precision machined from graphite with low salt and gas permeability. Maximum power was around 7.5 MW_{th} with heat rejection to the atmosphere.[4] MSRE was the first successful demonstration of liquid-fueled molten salt-cooled nuclear reactor technology, achieving >13,000 h of full power, and most of the major objectives were reached; it was the first reactor to run solely on ^{233}U from January to May 1969.[5] It had one of the highest core outlet temperatures (~662°C) for a nuclear reactor of its time. Hundreds of thousands of hours of loop testing were conducted during the years of the MSRE demonstration and continued through the early 1970s. From the years of MSRE operation and loop testing experiments, much information was gained about the material performance and compatibility of Ni-base salt-facing container alloy Hastelloy N (still one of the major candidate alloys for construction of advanced MSR designs today) and tritium behavior in molten salt, and also several grades of graphite were seal coated, corrosion tested and irradiated.

The advantages of thorium-based fuel cycles were recognized during the MSRE years.[5] Breeding fissile ^{233}U inventories from ^{232}Th as an alternative to enriched uranium fuel cycles is still an alluring concept, naturally for those countries that have significant thorium reserves like China,[6] India,[7] and the United States.[8] Both ^{238}U and ^{235}U are primordial radionuclides of U, and ^{232}Th is the only primordial radionuclide of Th. ^{232}Th, like ^{238}U which transmutes to fissile ^{239}Pu, is not fissile but a fertile radionuclide that gives birth to fissionable species via transmutation to ^{233}U. Th is four times more naturally abundant than U, and the use of Th-based fuel contributes significantly less to Pu stockpiles.

For MSRE, a thermal neutron spectrum appeared to have superior breeding ratios over intermediate or fast fluxes; very high power densities would be required to avoid excessive fissiles in a hard neutron spectrum.[9] Since there was limited moderation from salt constituents, a homogenous reactor core was eliminated from consideration in favor of a graphite-moderated core.[1] Two types of graphite-moderated breeder configurations were considered for $^{233}U/^{232}Th$: single-fluid where ^{233}U and ^{232}Th were contained in the same salt and two-fluid where the ^{232}Th was kept separated from the ^{233}U in seed and blanket regions of the core. Much of the fuel and coolant compositions for MSRE were later extended by ORNL to the 1000 MW_e breeder reactor concept in the 1970s known as the Molten Salt Breeder Reactor (MSBR).[10] The MSBR was envisioned to be a thermal spectrum reactor with a graphite-moderated

core that operated around 700°C and utilized a $^{232}Th/^{233}U$ fuel cycle using $^{7}LiF–BeF_2–ThF_4–UF_4$ (71.7–16–12–0.3 mol%) as the fuel salt mixture. A single-fluid design with chemical processing was envisioned because by this time, problems were anticipated with the two-fluid design with graphite piping; graphite irradiation behavior and dimensional change (see Section 4.09.4.2.2) were evident with prolonged exposures of graphite to high neutron fluxes. For the helium channels in between graphite assemblies, neutron flux gradients would lead to differential volume changes, and the channel swelling behavior would cause fuel salt "plumbing issues" due to changes in graphite volume fraction and relative volume change in the helium space.[11]

In 1969, the MSRE demonstration at ORNL was shut down after 4 years, but it was not due to technical infeasibility. MSRE was a very successful demonstration of MSR technology. In subsequent years, the MSBR research at ORNL progressed and reached a point of needing substantial funding but was terminated as well without a prototype demonstration. In the post-World War II era, the US Atomic Energy Commission was more interested in the liquid metal fast breeder reactor (LMFBR) using the $^{238}U/^{239}Pu$ cycle, for production of Pu. Compared to the MSRE/MSBR programs in which ORNL was the only stakeholder, the LMFBR program had gained significant nation-wide momentum at the time, received major federal funding and had many stakeholders.[5] MacPherson, who was first the director of the ORNL MSR program and later Deputy Director of the lab, wrote that "there was no interest in funding a competitor".[5]

4.09.1.2 Types of Molten Salt Reactors

Today, MSRs are one of six Generation IV (GenIV) advanced nuclear reactors for the Next Generation Nuclear Plants (NGNP). Superior to the current generation nuclear reactors, a GenIV reactor concept has to offer enhanced safety features, be economically competitive, generate less long-lived radioactive waste, have enhanced fuel efficiency as well as lower probabilistic risks of radioactive release to the environment. A typical MSR operates around 600–700°C at near atmospheric pressure. MSRs fall into one of two major design categories (although the first type is more common): (1) those where the molten salt is a coolant and solvent in a liquid-fueled reactor and (2) those where the molten salt is a coolant for a solid fueled-reactor. MSRs are fission reactors for electricity generation. They should also be distinguished from liquid metal cooled reactors, which are fundamentally different and not discussed in detail here. For the liquid-fueled MSRs, they can be further classified as breeder reactors or actinide burners (converters). As this article will reveal, there are many additional challenges with an MSR breeder reactor compared to a burner reactor configuration. The solid-fuel MSRs integrate the advantages of other reactor categories; strong analogies can be drawn to gas reactors because they use the same ceramic fuels. On the other hand, solid-fuel MSR breeders have probably not been proposed, because the chemical processing of fuel is much more feasible in the liquid phase.[1]

For the liquid-fuel MSR design, molten fluoride salts such as eutectic binary $LiF–BeF_2$ (also known as FLiBe) and ternary LiF–NaF–KF (also known as FLiNaK) salts are commonly preferred as the coolant and fuel solvent. Liquid fuel does not have to be developed separately or disposed of separately, so less waste is generated.[2] Liquid-fuel MSRs have the following technical advantages over solid-fueled MSRs: (1) a high negative temperature coefficient of reactivity, (2) liquid fuel burnup is not limited by radiation damage, (3) the potential for continuous fission product removal and (4) potential for continuous fuel makeup.[1] Fluoride salts are typically preferred for thermal and fast spectrum reactors because of their favorable thermophysical properties, neutronics and because there is prior experience with these salts. Chloride salts are only being considered for harder neutron spectrums due to the unfavorably high thermal neutron capture cross-section of ^{35}Cl ($\sigma_{th} = 35.3$ barns), and it typically needs to be separated from ^{37}Cl; both are stable Cl isotopes.[12] Neutron activation of ^{35}Cl chloride salt produces a gaseous, long-lived isotope, ^{36}Cl ($t_{1/2} = 3.01 \times 10^5$ y). Isotopes of Cl are readily dissolvable in water and their high mobility makes waste management more challenging[13,14]; pyro-reprocessing of liquid chloride salts to separate UCl_3 and $PuCl_3$ is a notable technical challenge.[13,14] In light of foreseeable Li shortages due to the battery industry and speculative market prices in the last decade, there are definite proponents of Cl-salt reactors. **Table 1** shows some MSR development activity by country.

Solid-fueled MSRs offer an overwhelming advantage over liquid fuel designs, because they do not require the same chemical processing of the fuel. In the same vein, solid fuel reactors do not make practical breeders because of the difficulty of processing the fuel. Solid fuel MSRs have more recently emerged as the Advanced High Temperature Reactor (AHTR), which are sometimes described as a salt-cooled Very High Temperature Reactor (VHTR) because of the intersection of MSRs and High Temperature Gas-Cooled Reactors (HTGR) that use the same ceramic fuel. Subsequently, the Fluoride Salt-Cooled High Temperature Reactor (FHR) concept originally proposed by UC-Berkeley,[15–17] is a type of AHTR using a non-fueled molten fluoride salt coolant and the same solid fuel as VHTRs. FHRs rely on several, diverse classes of heat resistant materials[18] including refractory ceramics (silicon carbide composites, carbon composites, etc.) and metallic alloys (Hastelloy N, Type 316H stainless steel, etc.) along with a graphite-moderated core.[16] FHRs benefit from utilizing maturing tri-isotropic structural (TRISO) fuel technology that offers a large safety margin ($T_{max} \sim 1600$°C). Additionally, the fuel pebbles are cycled through the system several times to maximize fuel burnup and they are replaceable once depleted, and most fission product gases are retained within the TRISO containment layers of the silicon carbide (SiC), pyrolytic carbon (PyC) and graphitic matrix carbon that overcoat the fuel kernel. Since the U is typically in the form of a solid oxide or carbide compound and encapsulated in these layers, there is no additional challenge of dissolving fuel into molten salt.

For NGNP, the two GenIV MSR baselines are the Molten Salt Fast Neutron Reactor (MSFR) and the AHTR (FHR falls in this category). Among the many GenIV initiatives satisfied by both designs, fast reactors make good breeders and converters. Typically, to burn TRU waste, a fast neutron spectrum is required because of the low fission probabilities of TRU in thermal reactors (but see ThorCon in **Table 1**, proposing an MSRE "scale-up"). Fast reactors do not require the same chemical processing of salt like thermal

Table 1 Current liquid-fueled and solid-fueled MSR development by country

Country	*Reactor*	*Neutron spectrum*	*Fuel format*	*Molten salt*
USA	Berkley FHR	Thermal	Solid – pebble bed TRISO-based	FLiBe/FLiNaK
USA	FHR-KairosPower	Thermal	Solid – pebble bed TRISO-based	FLiBe/FLiNaK
USA/Canada	MCSFR-Elysium (loop)	Fast (actinide burner)	Liquid-TRU[a] based	Cl-salt
	MCSFR-Elysium (modular)	Fast (actinide burner)	Liquid-TRU based	Cl-salt
USA	MCFR-TerraPower	Fast (actinide burner)	Liquid – proprietary	Cl-salt
USA	"TAP" – Transatomic Power	Thermal/Epithermal (actinide burner)	Liquid-LEU-based	LiF-(Act.)F_4
USA/Canada	IMSR – Terrestrial Energy	Thermal (actinide burner)	Liquid – LEU or SEU[b]-based	Fl-salt
Denmark	MSR "CUBE" – Seaborg	Varies spatially (actinide burner)	Liquid – Th based	Fl-salt
Russia	MSFR "MOSART"	Fast (actinide burner)	Liquid – TRU based	FLiBe
France	MSFR	Fast (breeder)	Liquid Thorium-based	FLiBe
Indonesia	"ThorCon"	Thermal (actinide burner)	Liquid-Th/U	$NaBeF_4$-salt
China	TMSR-SF	Thermal	Solid – TRISO-based	FLiBe/FLiNaK
	TMSR-LF	Thermal (breeder)	Liquid – closed Th/U fuel cycle	FLiBe/FLiNaK
	TMSRF-LF	Fast (actinide burner)	Liquid – TRU based	FLiBe/FLiNaK

[a]Transuranic waste from LWR spent nuclear fuel. Integrated Molten Salt Reactor.
[b]Slightly-enriched uranium typically having concentrations of 1 to 2% ^{235}U.
Note: Molten Salt Reactors. (accessed 06.11.19) Available at: http://www.world-nuclear.org/information-library/current-and-future-generation/molten-salt-reactors.aspx. Forsberg, C.W., 2007. Thermal- and Fast-Spectrum Molten Salt Reactors for Actinide Burning and Fuel Production, ANS Manuscript Number 175768. Smith, N.V., 2017. Presentation: MSR TWG Licensing Perspective. NRC DOE Workshop on Advanced Reactors. (accessed 06.11.19) Available at: https://www.nrc.gov/docs/ML1713/ML17135A131.pdf.

reactors. Fast un-moderated breeder reactors, although the initial core still relies on substantial fissile loads (starter fuel) of enriched U or Pu, can utilize either the $^{233}U/^{232}Th$ or $^{238}U/^{239}Pu$ cycles and can burn TRU waste from Light Water Reactors (LWR). LWRs comprise more than 80%[19] of the world's current generation reactors; Pu and minor actinides are produced from LWRs contributing annually to civilian stockpiles of Pu worldwide. It is no wonder why three of the six GenIV reactor concepts are fast reactors with varying degrees of technical readiness. A Th-based fuel cycle produces significantly less Pu and high-level actinides. At least in the US, there is no license yet to use Th fuel in civilian reactors. Although the US Nuclear Regulatory Commission (NRC) with the advice of ORNL has released a report in NUREG/CR-7176[20] on the gaps in licensing assessment of Th fuel, it applies to mixed oxide (MOX) fuels in LWRs.

4.09.1.3 Fusion and Non-MSR Concepts

Molten salts have also been applied to non-MSR nuclear applications like the liquid salt-cooled solid-fuel fast reactor (LSFR), blanket salt to breed tritium in future fusion reactors, such as the fusion-fission hybrid reactor (FFHR-2) at the National Institute for Fusion Sciences in Japan,[21] and as liquid structures for protection of heavy ion fusion target chamber walls and magnets from neutron irradiation.[22] In magnetic fusion energy (MFE) reactor designs, FLiBe has been considered as a plasma-facing material and as a tritium-breeding coolant. In inertial fusion energy (IFE) designs, FLiBe was selected as the working fluid for thick liquid wall protection jet arrays in the Heavy Ion Fusion (HIF) reactor concept due to its ability to absorb fusion neutrons and protect structures in the target chamber from ablation by target X-rays, debris and radiation damage.[22] The Laser Inertial Fusion Energy (LIFE) concept uses TRISO fuel and FLiBe. Corrosion in these systems is also managed by maintaining a low fluoride potential in FLiBe as is the case for MSRs. For MFE, PbLi was selected over FLiBe for the US and international fusion research efforts, but some critical R&D activities were still pursued prior to 2007 to investigate the tritium breeding, chemical compatibility, redox control, and heat transfer capabilities of FLiBe through the JUPITER-II US DOE/Japan MEXT collaboration.[23,24]

It is difficult to ignore the favorable thermophysical properties of molten fluoride salts, as shown in **Table 2**, compared to other coolants which allow for the potential for higher thermal efficiency in MSRs. Compared to HTGRs/VHTRs, better heat transfer characteristics of molten salt compared to helium results in high thermal efficiency, thus significantly lowering pumping costs and capital costs (smaller heat exchangers, compact construction, less piping, etc.). **Table 2** compares the thermophysical properties of various coolants in LWRs, HTGRs/VHTRs, MSRs, and SFRs.[25–27] Coolant melting points are very decisive. The LSFR concept was proposed by researchers in the US and France to replace sodium in sodium fast reactors (SFR) with clean, non-fueled molten salt. For instance, outlet temperature of SFRs could be increased from 500 to 550°C (for sodium) to 700–750°C (molten fluoride salt), with corresponding increases in plant efficiency from 42% to about 50%.[28] The LSFR is like an integrated MSR concept because it borrows the molten salt coolant, but SFRs are fundamentally different GenIV concepts from GenIV MSRs and are not elaborated further.

Compared to other coolants and molten salts ($KF–ZrF_4$ and $NaF–NaBF_4$), FLiBe has several advantages. For example, like light water, FLiBe has a very high volumetric heat capacity, and it is transparent. It is composed of low-Z elements and provides some neutron moderation. One drawback could be that FLiBe has a high melting point relative to other coolants. Another technical drawback of FLiBe (see Section 4.09.2.2 for additional hazards with Be-bearing salts) is that ^7Li enrichment of FLiBe is required to make it viable as a primary coolant because of the significant thermal neutron capture cross-section of ^6Li ($\sigma_{th} = 490$ barns).

Table 2 Coolants and their thermophysical properties, measured, and extrapolated from literature

Coolant	T_{mp} (°C)	T_{boil} (°C)	ρ (kg/m^3)	C_p (kJ/kg °C)	$\rho\ C_p$ (kJ/m^3 °C)	k (W/m °C)	$v \cdot 10^6$ (m^2/s)
FLiBe (700°C, 0.1 MPa)	459	1430	1940	2.42	4670	1	2.9
FLiNaK (700°C, 0.1 MPa)	454	1570	*2019*	0.45	*909*	*0.9*	–
58.0%KF–42.0%ZrF_4 (700°C, 0.1 MPa)	390	1450	*2795*	*0.251*	*702*	*0.39*	–
8.0%NaF–92.0%$NaBF_4$ (700°C, >0.1 MPa)	385	700	1750	1.51	2640	0.5	0.5
Sodium (550°C, 0.1 MPa)	97.8	883	820	1.27	1040	62	0.12
Lead	328	1750	10,540	0.16	1700	16	0.13
Helium (7.5 MPa)	–	–	4	5.2	20	0.29	11
Water (290°C, 7.5 MPa)	0	290	732	5.5	4040	0.56	0.13

Note: Ambrosek, J., Anderson, M., Sridharan, K., Allen, T., 2017. Current status of knowledge of the fluoride salt (FLiNaK) heat transfer. Nucl. Technol. 165 (2), 166–173. Wilson, D., 2006. Assessment of Candidate Molten Salt Coolants for the NGNP/NHI Heat Transfer Loop. ORNL/TM-2006/69. Wilson, D., Toth, L.M., Clarno, K.T., 2006. Assessment of Candidate Molten Salt Coolants for the Advanced High-Temperature Reactor (AHTR). ORNL/TM-2006/12.

Neutron capture reactions, Reactions 1–3, and positron decay in Reaction 4 illustrate the potential pathways by which tritium can be continually produced from FLiBe activation, despite initial enrichment.[29]

$$^{6}_{3}LiF + {}^{1}_{0}n(thermal) \rightarrow {}^{3}_{1}HF + {}^{4}_{2}\alpha \quad (1)$$

$$^{7}_{3}\mathrm{LiF} + {}^{1}_{0}n(fast) \rightarrow {}^{3}_{1}HF + {}^{4}_{2}\alpha + {}^{1}_{0}n' \quad (2)$$

$$^{9}_{4}\mathrm{BeF_2} + {}^{1}_{0}n \rightarrow {}^{4}_{2}\alpha + {}^{6}_{2}He + 2F \quad (3)$$

$$^{6}_{2}He \rightarrow {}^{6}_{3}Li + e^{+} + \gamma_e(\mathrm{t}\,½ = 0.8\ \mathrm{s}) \quad (4)$$

Compared to the current fleet of more than 400 commercial LWRs worldwide and 15 gas-cooled reactors in the UK and Russia, MSRs offer overwhelming safety and economic advantages as a low-pressure system. MSRs will not generate large volumes of steam containing radionuclides, and molten fluoride salts do not react violently with water. Criticality accidents and core meltdown are unlikely with MSRs because there is little excess reactivity, and the molten salt is designed to drain into critically safe storage in the event of a SCRAM.[16]

4.09.2 Choice of Fuel and Coolant Salts

The selection of salt for a specific application depends on the: (1) type of MSR (breeder, actinide burner, solid-fueled, etc.), (2) the purpose of the salt (coolant, liquid fuel/coolant, heat transport, etc.), (3) melting points (beneficial thermal properties in the liquid state) and (4) corrosivity (chemical compatibility with reactor materials of construction). Other considerations include feedstock availability/sustainability, waste management, and environmental issues. In old MSRE technical reports, it was not the fissile or fertile components of the fuel salt (0.2–1 mol% U) but the salt itself that drove costs. Other than hydrofluorination, further purification of molten fluoride salt was not feasible at the time, so the only realistic option was to buy the purest salt constituents.[30]

4.09.2.1 Selection of Salts for Reference MSR Concepts

The first fuel salts for ARE, MSRE and MSBR designs were chosen based on the following criteria[30]: (1) low neutron cross-section, (2) thermal stability of salt components, (3) low vapor pressure, (4) radiation stability, (5) adequate solubility of fuel (including TRU from spent nuclear fuel), (6) adequate heat transfer and hydrodynamic properties, (7) chemical compatibility with container and moderator materials, and (8) low fuel and processing costs.

Diluents were selected by capture cross-sections and stability of diluent fluoride compounds towards reduction by common structural metals (Cr, Fe, Ni, etc.).[30] **Table 3** shows thermodynamic data and thermal neutron cross-sections for the formation of diluent fluoride compounds around 1000K for most compounds listed.[30] Metal fluoride mixtures are used to keep melting points as low enough for practical use. For the case of BeF_2, which has a very low capture cross-section and useful melting point, it cannot be used by itself because of its high viscosity[30]; in FLiBe, LiF, and BeF_2 form a eutectic, and LiF significantly lowers the resulting viscosity of the mixture.[30] If considering just the nuclear properties of compounds in **Table 3**, Be, Bi, ^{7}Li, Pb, Zr, Na, and Ca are preferred in order.[30] Elements with low thermal neutron cross-sections shown in **Table 3** are preferred for major salt constituents. Based on the **Table 3** data, salts that would contain easily reducible cations (Bi^{3+} and Pb^{2+}) were rejected because they would not be stable in nickel or iron-base alloys of construction.[30,31] The general rule for testing stability of materials of construction with salt is approximated by the standard molar Gibbs free energy of formation ΔG_f, shown in **Table 3** for fluoride compounds of salt, fuel, and container material (provided in both SI and non-SI units); in some cases the values should just be used as approximations as they originate for solutions in molten mixtures. The transition metal fluorides of interest at 1000K, fall within in -74 to -58 kcal/mol of

Table 3 Approximate Gibbs free energy of formation of fluoride compounds at 1000K, populated from various sources

Fluoride compounds in solid state	*ΔG_f, 1000K[a,b] (kJ/mol of F)*	*(kcal/mol of F)*	*Melting point (°C)*	*Thermal neutron cross-section (barns)*
Diluents				
CaF_2	−523	−125	1418	0.43
LiF	−523	−125	910	0.18
BaF_2	−519	−124	1368	1.17
SrF_2	−515	−123	824	0.17
YF_3	−473	−113	1290	0.23
MgF_2	−473	−113	848	0.033
NaF	−469	−112	727	0.032
KF	−456	−109	1387	1.27
BeF_2	−435	−104	1263	0.063
ZrF_4	−393	−94	995	0.53
AlF_3	−377	−90	858	1.97
PbF_2	−259	−62	554	0.01
BiF_3	−209	−50	649	0.032
Structural metals				
CrF_2	−310	−74[a]	1100	3.1
FeF_2	−278	−67[a]	930	2.5
NiF_2	−243	−58[a]	1330	4.6
Active fuel constituents				
PuF_3	−692	−166[b]	1396	–
CeF_3	−494	−118[c]	1477	–
ThF_4	−423	−101[a]	1111	–
UF_3	−420	−101[a]	1495	–
UF_4	−397	−95[a]	1036	–

[a]Ref. 30.
[b]at 715°C, Refs. 34,32,33.
[c]Ref. 35.

F atom. Thus, standard molar free energy ΔG_f changes higher (more negative) than this value would help assess which materials will be stable with respect to the salt.

Major actinides U and Pu and minor actinides Th and Ce along with most fission products (like Cs and I) readily dissolve into the salt to form stable fluoride compounds (see **Fig. 1** and **Table 3**) that remain in the molten salt mixture until they are chemically separated; compounds like CsI are also known to form. Noble gases (like Xe and Kr) are known to be relatively insoluble in molten fluoride salt.[10,31] In **Fig. 1**, the relative stability of fluoride compounds is indicated approximately by their enthalpy of formation per mole of fluorine;[31] the free energy for this reaction should vary in a similar way as the heat of formation other than some minor contributions from entropy and heat capacities. Alkali metals (Group II), alkaline earth metals (Group III) and tetravalent actinides (Th, Pa, U, Pu) and trivalent actinides tend to have standard heats of formation more negative than −95 kcal/mol of fluorine. The transition metal elements common in structural metals (Cr, Fe, Ni) generally have heats of formation (ΔH_f) between −100 and −80 kcal/mol of fluoride. Relative to the transition metal fluorides the MSRE/MSBR salt constituents LiF and BeF_2 were perceived to be considerably more thermodynamically stable, and reaction between fuel salt components ThF_4, UF_4, PuF_3, PuF_4, etc., and metal were not favored to an appreciable extent.[31] Trivalent Pu and minor actinides tend to be the only stable species in various molten fluoride salts. PuF_3 solubility in a wide variety of salt systems is summarized in **Table 4** from various sources.

4.09.2.2 Fluoride Salts

Liquid-fueled systems face the additional challenge of adequate actinide solubility (including TRU waste). A liquid-fueled, thermal (epithermal) MSR breeder reactor utilizing a $^{232}Th/^{233}U$ cycle requires a driver fuel of fissile material (typically Pu) since ^{232}Th is not fissile itself. ^{232}Th gives birth to ^{233}U, but fissile inventories must first be built. PuF_3 drivers were researched and considered as early as the MSRE/MSBR[30,36] era at ORNL but also recently.[42] It is fortunate to have the potential to utilize Pu as a starter fuel for a Th breeder reactor that produces far less lifetime Pu than any LWR. Reactor-grade Pu has more rigorous handling requirements, including foreseeably tougher licensing issues and regulatory requirements; at least in the US, there is no license yet to use Th-based fuel. TRU solubility is also of great interest as some MSR concepts can be refueled with additions of TRU-Th based fuel.

Five classes of molten salt systems in **Table 4** possess usefully low melting points between 315 and 565°C while also having potentially viable neutronics and material compatibility with structural alloys: (1) alkali metal fluorides, (2) BeF_4-containing, and (3) ThF_4-containing, (4) ZrF_4-containing, and (5) BF_4-containing (fluoroborates) salts. For U or Th, they form a range of

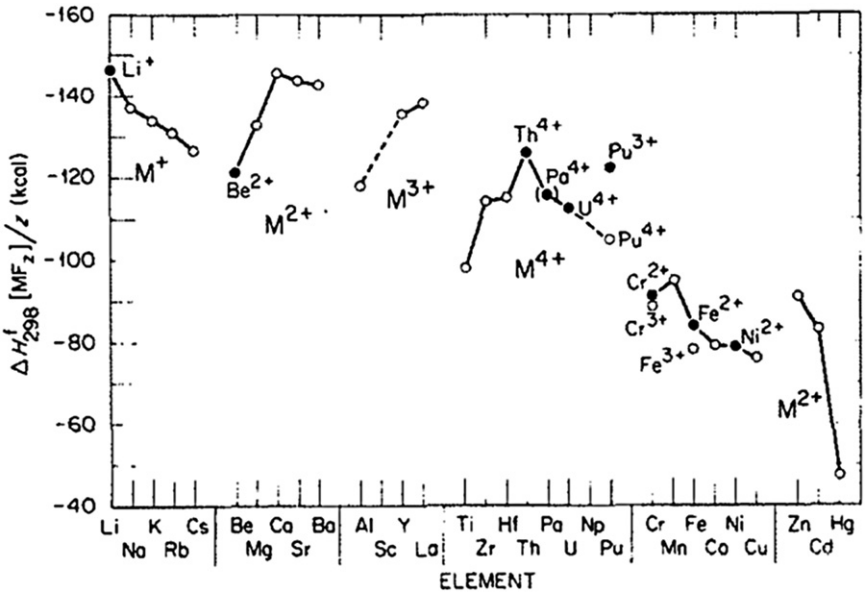

Fig. 1 Relative stability of fluorides from MSRE/MSBR by molar enthalpies of formation of crystalline metal fluorides $M^+ + F^- = M_xF_y$. Extracted from Baes Jr., C.F., 1974. Chemistry and thermodynamics of molten salt reactor fuels. J. Nucl. Mater. 51, 149–162.

compositions in which the salt will be completely molten with concentrations of active fluorides UF_4 and ThF_4 >10 mol% at 500°C and >20 mol% at 560°C.[36] Minor actinides and Pu^{3+} (and possibly Pu^{4+}) are among the only stable species in a wide range of salt systems in **Table 4**. Reduction of LiF and CeF_3 or PuF_3 are important for fuel reprocessing for MSBRs and is discussed in Section 4.09.3.2.

For Be-bearings salts like FLiBe, although very well-studied in the past, current knowledge of Be toxicity requires similar studies to continue with extra layers of scrutiny, including legal and administrative safety protocols when handling this known carcinogen. Be is a light, metallic element. BeO and most Be salts can dissolve into water and enter the human body through inhalation/ingestion of Be metal dust, mist, or contact with skin. Contamination, especially fine particulate Be metal dust that could become airborne, could be a serious problem that requires immediate remediation under federal regulations.[43] The most common health effects associated with overexposure to Be in occupational settings include Be sensitization, lung cancer and chronic beryllium disease.[43] To conduct FLiBe studies, the Be-bearing salt and specimens, Be-cleaning equipment and instruments would have to be a part of a dedicated Be facility, e.g., inside air-locked glove boxes. To deem a specimen safe to handle post-test requires testing for Be with swabs to ensure allowable Be contamination limits are not exceeded. There are not many facilities or laboratories that will risk contamination of their analytical instruments with this hazardous chemical. Thus, there is a notable impact on the number of actual experiments with material performance in FLiBe. Sometimes FLiNaK is used as a non-toxic surrogate for FLiBe corrosion studies, but because of its excess F content, it is debatable whether FLiNaK results are relevant.

Fluoroborates (BF_4-containing) salts were considered for MSRE/MSBR secondary coolant salts. An iterative process to identify the right diluent and additives ensued for several years with extensive irradiated capsule and loop compatibility testing of materials. While coolant salts like NaF–ZrF_4 and FLiBe were valued for their excellent compatibility with Hastelloy N, the high costs of the salts (especially those LiF-based) motivated other options.[30,44] On the basis of low cost (about $0.50/lb at the time) and a relatively low melting point (around 400°C to facilitate heat transfer to supercritical steam), fluoroborates like $NaBF_4$ in particular, with a small amount of additives like NaF and or KBF_4 were proposed before testing their corrosivity towards reactor materials. NaF–$NaBF_4$ forms a eutectic around 60 mol% $NaBF_4$ which melts at ~384°C.[44] In case NaF–$NaBF_4$ was deemed unsuitable, other backup options were NaF–KF–BF_4, with the potential for freezing points below 700°F and BeF_2 options (NaF–BeF_2,[36,45] NaF–LiF–BeF_2[36,45]) or KF–ZrF_4–AlF_3[46] because these salts were shown to be compatible with Hastelloy N.[30] Substitution of ZrF_4 or even AlF_3 for some of the BeF_2 was attempted to lower the viscosity of mixtures without a penalty to the liquidus temperature of these melts. The ZrF_4 was added also to eliminate the possibility of UO_2 precipitation, although it was later concluded during MSBR conceptualization that oxides would be removed by chemical processing of the fuel salt (see Section 4.09.3.2).

Adequate Pu solubility for actinide burning has been researched with CeF_3, a proxy compound for PuF_3 in MSFR actinide burner configurations due to their similar properties, except CeF_3 has the advantages of being more available, and CeF_3, ThF_4, and LiF have less hazardous handling issues. Capelli *et al.*[42] determined CeF_3 solubility in various molten fluoride melts in **Fig. 2** and affirmed that CeF_3 can be a proxy for PuF_3 in LiF–ThF_4.

The solubility of PuF_3 is high in these salt systems relative to that of ZrF_4, UF_4, UF_3, and ThF_4. PuF_3 solubility is at a maximum (~20%) in pure LiF, NaF, of KF and decreases with addition of BeF_2 and ThF_2.[37–40] From **Table 4**, the LiF–PuF_3 system forms a eutectic with 20 mol% PuF_3 at 743°C.[37] The calculated solubility of PuF_3 in the matrix of LiF–NaF–KF (46.5–11.5–42 mol%) at

Table 4 Molar composition of calculated solubility of PuF_3 by in a wide variety of salt systems and temperatures

Chemical formula	*Molar composition*[a] *(%)*	T_{mp} *(°C)*	*Solubility of* PuF_3[b] *(mol%)*
Alkali-metal fluoride-containing			
LiF–PuF_3	80:20 eutectic	743[c]	20[c]
LiF–NaF–KF	46.5:11.5:42	454	19.3[d]
LiF–KF	50:50	492	–
LiF–RbF	44:56	470	–
LiF–NaF–RbF	42:6:52	435	–
BeF_2-containing			
LiF–BeF_2	73:27	530	2.0[e]
	66:34	458	0.5[e,f]
LiF–NaF–BeF_2	15:58:27	479	2.0[e,f]
	31:31:38	315	0.4[e]
LiF–BeF_2–ZrF_4	64.5:30.5:5	428	–
NaF–BeF_2	57:43	340	0.3[e]
ThF_4-containing			
LiF–ThF_4	78:22	565	4.2[g]
LiF–BeF_2–ThF_4	75:5:20	560	3.1[g]
	71:16:13	499	1.5[g]
	64:20:16	460	1.2[g]
	47:51.5:1.5	360	–
LiF–ThF_4–PuF–UF_4	73:21:1:5	646[h]	1.0
ZrF_4-containing			
NaF–ZrF_4	59.5:40.5	500	1.8[f]
LiF–ZrF_4	51:49	509	–
LiF–NaF–ZrF_4	42:29:29	460	–
	26:37:37	436	–
NaF–RbF–ZrF_4	10:48:42	385	–
KF–ZrF_4	58:42	390	–
BF_4-containing			
KF–KBF_4	25:75	460	–
RbF–$RbBF_4$	31:69	442	–
NaF–$NaBF_4$	8:92	384	–

[a]Ref. 36.
[b]Solubility data reported around 600°C.
[c]Ref. 37.
[d]Ref. 38.
[e]Ref. 39.
[f]Ref. 40.
[g]Ref. 41.
[h]Ref. 42.

600°C was 19.3 mol%.[38] In **Table 3**, thermodynamic considerations of a large negative Gibbs free energy of PuF_3 found by Bamberger in 1970[34] at 1000K relative to other active fluorides allows one to perceive PuF_3 formation as very favorable at those conditions. Adequate solubility of PuF_3 at 600°C in burner concepts (~0.2 mol%) can be achieved using LiF–NaF–BeF_2 and breeder fast-spectrum concepts (3–4 mol%) can be achieved using LiF–BeF_2–ThF_4 fuel solvent systems as shown in **Table 4**. The CeF_3 and PuF_3 solubilities in LiF–ThF_4 were reproduced very well by a thermodynamic model in **Fig. 2** against the same experiment data set by different authors.[35,42] These studies affirmed that ThF_4 could be a proxy for UF_4 because of its minimal effect on fuel salt properties after partial substitution of UF_4 with ThF_4.

4.09.2.3 Chloride Salts

Another important group of salts, not mentioned in **Table 4** because of the scarcity of data and potential discrepancies, are chloride salts. Overall, chloride salts have less technical advantages than fluoride salts but they have lower melting points, thus a higher actinide solubility at lower temperature, making them ideal for fast TRU burner configurations.[47,48] Another advantage of chloride salts is avoidance of Li enrichment and Be toxicity. Interestingly, the earliest known UCl_3 and UF_4 thermochemical data, eutectic temperature and phase relations in various salt systems for the purposes of electro-separation were collected and determined in 1943 by the well-known chemist Charles A. Kraus (an advisor to the Manhattan Project)[49] and also in 1959 by Thoma[36] at ORNL. In the 1960s, Brookhaven National Laboratory (BNL) performed 10,000s of hours of corrosion tests of various stainless steels

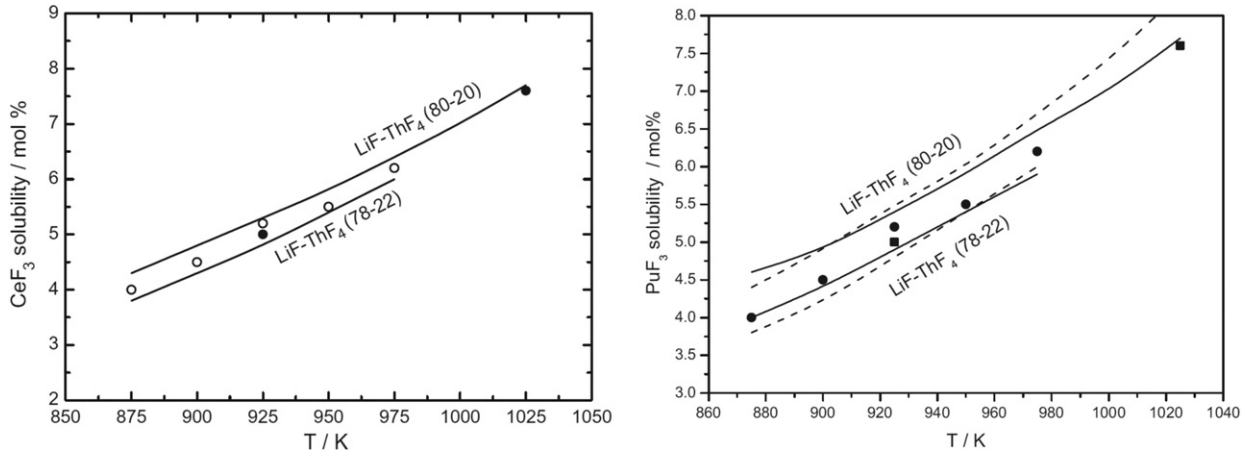

Fig. 2 (Left) Solubility with temperature of CeF_3 in LiF–ThF_4 modeled against experimental data in two different LiF–THF_4 (80–20 mol%) nominal compositions (Right) PuF_3. Reproduced from Beneš, O., Konings, R.J.M., 2013. Thermodynamic assessment of the LiF–CeF_3–ThF_4 system: Prediction of PuF_3 concentration in a molten salt reactor fuel. J. Nucl. Mater. 435 (1–3), 164–171. Capelli, E., Beneš, O., Konings, R.J.M., 2015. Thermodynamic assessment of the LiF–ThF_4–PuF_3 –UF_4 system. J. Nucl. Mater. 462, 43–53.

exposed to chloride salts in thermal convection loops (TCL) using LiCl–KCl eutectic salt and in loops using NaCl–KCl–$MgCl_2$ (30–20–50 mol%) eutectic salt. Around 2006, Mourogov and Bokov proposed a fast MSBR, REBUS-3700, that utilized UCl_3 and $PuCl_3$ in a liquid NaCl matrix.[50] Argonne National Laboratory (ANL) developed a $UCl_3/PuCl_3$ separation scheme as a part of their Integral Fast Reactor (IFR) program.[51,52] TerraPower is developing the molten chloride fast reactor (MCFR).[53] Researchers have contributed thermodynamic evaluations for UCl_3 solubility[13,47,48] and corresponding experiments[13] in various salt systems recently but material corrosion data[14,54] is still limited for chloride salts. Pu handling creates some obvious regulatory issues so some CeF_3 surrogate studies are underway.[47] Some recent assessments of NaCl–UCl_3–$CeCl_3$ tend to show discrepancies in the liquidus curve of the fuel salt system (up to 30–40°C increase in some compositions[47]), which is crucial to determining the minimum operating temperature of the entire core and preventing precipitation of TRU material.

Chloride salts are proposed for LSFR concepts like the 2400 MW_{th} liquid salt-cooled, flexible-conversion-ratio reactor, utilizing coolant salt NaCl–KCl–$MgCl_2$ (30–20–50 mol%).[55] The maximum cladding temperature is projected to be 650°C.[55] Compared to sodium used in fast reactors, the base case chloride salt for this reactor has a melting point of 396°C. The general consensus from LSFR studies is that chlorides are less stable than fluoride salt mixtures, and they are more corrosive towards reactor materials, but this needs further research and development for MSRs. For instance, sulfur from ^{35}Cl and fission products have the potential to precipitate, which can create additional challenges in processing. For LSFR, KCl–$MgCl_2$ is proposed as a heat transfer fluid, along with candidates LiF–NaF–KF and KF–KBF_4, for coupling a reactor with a chemical plant or a hydrogen production facility. KCl–$MgCl_2$ has the potential to be very low-cost. BNL studied chloride salts LiCl–KCl and NaCl–KCl–$MgCl_2$ (30–20–50 mol%) eutectic salt with stainless steels in thermal and forced convection loops in the 1960s,[56] but these loop tests refer to LMFBRs which are non-MSR concepts and will not be elaborated here.

4.09.3 Developments in Salt Preparation and Purification

Salt preparation typically begins with the acquisition of raw components that when combined and heated form a molten mixture that reflect some combination of the component properties. However, most vendors of halide salts do not provide materials that can be used immediately. Moisture-based contaminants tend to be persistent in the process of forming, handling, testing and storage of salt in sealed containers. Aggregated data sets across different molten salt purification methods in corrosion experiments tends to show empirically that salt purification matters, whether it is purified in a liquid or solid form, what kind of purifying gases are used and how the salts are stored and handled, etc.[57] There is considerable scatter in laboratory results. This is also a result of a lack standardized corrosion testing of materials in molten salt.[57]

Corrosion of structural materials depends largely on the redox condition of the salt, which in fluoride salt, is defined as the fluorine potential (we use the term "redox" throughout this work, as it is more common).[58] The redox condition is defined as the oxidizing or reducing power of the salt depending on the electrochemical balance of the system. Maintaining a reducing salt environment helps to mitigate the dissolution of Cr. For U-based liquid fuels, the redox potential is typically controlled by the ratio of UF_4 to UF_3. It has been shown that the redox condition of the salt can be made less oxidizing by maintaining a minimum amount of UF_3 in addition to the UF_4.[59–62] Baes recommended maintaining a ratio of UF_4/UF_3 (often also written as U^{4+}/U^{3+}) between 10 and 100 to control corrosion in the MSRE.[31] Olander classified redox control into three major categories: (1) gas phase control, (2) major metal control, and (3) dissolved salt control.[58] An example of major metal control is adding metallic Be to the melt.[60,63] Major metal control using Be

to maintain the U^{4+}/U^{3+} will not apply to FHR because fissile species should not be present in the primary coolant. Applying an Eu^{3+}/Eu^{2+} couple, using Gd as a reducing agent for redox control could be feasible for the second salt loop of FHR.[64]

4.09.3.1 Salt Purification Methods

During the MSRE/MSBR programs, considerable effort was devoted to salt purification by hydrofluorination with HF/H_2, which is described in numerous reports.[65–67] In addition to removing moisture/oxide impurities, the purification also removes other halide contaminants such as chloride and sulfur. Sulfur is usually present in the form of sulfate and is reduced to sulfide ions, which are swept out as H_2S in the sparging operation. Methods were also developed to ensure the purity of the reagents used to purify the salts and clean the container surfaces used for corrosion testing. Another means of purification that can be performed after sparging involves simply reducing the salt with a constituent active metal such as an alkali metal, beryllium, or zirconium. While such active metals will remove oxidizing impurities such as HF, moisture, or hydroxide, they will not affect the other halide contaminants that influence sulfur removal. Therefore, it seems inevitable that the HF/H_2 sparging operation, either by itself or followed by a reducing (active metal) treatment, will be a necessity. Although a great deal of effort can be devoted to purify the molten salt mixture in the manner described above, it is primarily useful in producing materials for research purposes, without the possibility of interference from extraneous impurities.

Removal of oxygen containing impurities form chloride and fluoroborate salts is considerably more difficult because the fluoride ion more readily displaces oxygen from most compounds than does the chloride ion, and because borate and hydroxyborate impurities are difficult to remove by fluorination with HF. Nearly all of the chloride salts prepared for corrosion studies have had relatively high levels of oxygen-containing impurities.[57] The typical salt preparation for these studies involved treatment of reagent chlorides by drying the solid salt under vacuum, followed by prolonged treatment with dry HCl gas, and finishing with an inert gas purge of HCl from the salt. This treatment is not effective in removing the last portion of bound oxygen from the salt. Depending on the salt composition, oxygen contents of up to a few percent (in wt%) may remain. A more effective method for removing oxygen is needed to investigate the basic corrosion mechanism in pure chloride salts; otherwise, the effects of oxygen-containing species will dominate the apparent corrosion response. The use of carbochlorination has been recommended for the removal of oxygen and it has been claimed that salts with very low oxygen content ($\sim$3 ppm) can be produced by this method.[68,69]

Initial purity and purification methods as well as unpurified salts tend to exhibit significantly different corrosion rates in laboratory tests.[57] For example, Indacochea *et al.* at ANL studied corrosion rates of stainless steel and nickel alloy samples in chloride salts.[70] The salt was sparged with pure Ar. In another work by the same author,[71] the salt was bubbled with an Ar-oxygen mixture. The oxygenated salt was much more corrosive, and the sample dissolved completely in 725°C for 720 h. Ambrosek[72] conducted 24 h exposures in $KCl–MgCl_2$ with different purification treatments and found samples exposed to salts treated with solid Mg or sparged with CCl_4 exhibited less mass loss than samples in salt sparged with HCl or pure Ar.

4.09.3.2 Chemical Processing of Fuel Salt

In a liquid breeder reactor some fission products like ^{233}Pa interfere with breeding, are bad for neutronics ^{135}Xe ($\sigma_{th} \sim 2$ million barns) or are gaseous like tritium with high mobility through graphite and structural alloys. It was realized early in the MSRE/MSBR era that the ^{233}Pa isotope can disrupt breeding operations due to parasitic capture of 2 neutrons/atom of Pa and thus requires robust chemical processing technology to remove trace amounts of it relative to larger amounts of U and/or Th from a neutron flux.[31,73] ^{233}Pa is formed from the following nuclear reactions illustrated in Fig. 3. In the conversion chain of ^{232}Th to ^{233}U, ^{233}Pa is formed as an intermediate, and it is a neutron poison ($\sigma_{th} = 39.5$ barns). Compared to its counterpart in the uranium fuel cycle ^{239}Np ($t_{1/2} \sim 2.4$ days), ^{233}Pa has a relatively longer half-life ($t_{1/2} \sim 27$ days). During this period, ^{233}Pa would absorb a significant number of neutrons due to its high thermal neutron cross-section and transmutes to a non-fissile isotope ^{234}U ($\sigma_{th} = 100$ barns) instead of fissile ^{233}U. Thus, storage and decay time of at least 12 months (more than 10 half-lives of ^{233}Pa) was proposed, prior to processing, to ensure decay of ^{233}Pa to ^{233}U and minimize losses of ^{233}U fissile inventory.

PaF_2 is a soluble metal fluoride in a FLiBe-based salt system. In contrast, Pa_2O_5 is quite insoluble, and PaF_2 can be selectively converted to Pa_2O_5, which is a separable insoluble oxide. The idea of selective precipitation of Pa_2O_5 is the basis for several older MSR-related patents for removing ppb levels of ^{233}Pa (i.e., Refs. 73,74). Inorganic metal oxide precipitants should also be chosen

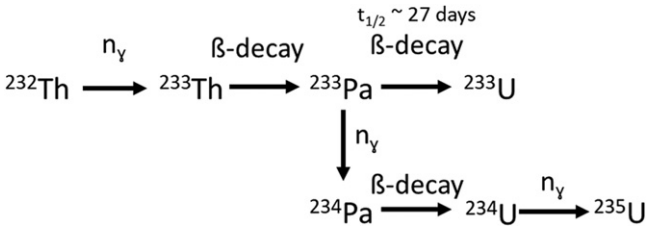

Fig. 3 Neutron capture by ^{232}Th to yield ^{233}Th. Then by ß decay, ^{233}Th converts to ^{233}Pa. If removed ^{233}Pa eventually decays to fissile ^{233}U but if not removed it can participate in double capture reactions and form ^{235}U.

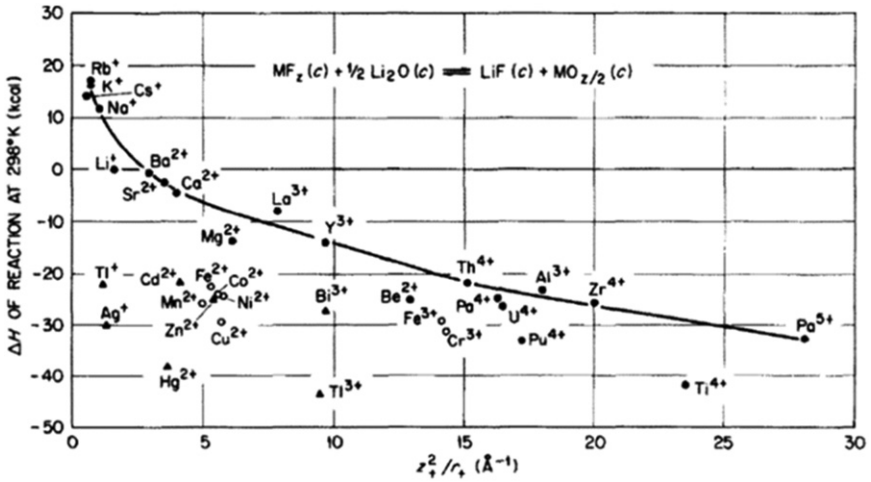

Fig. 4 Effect of cation charge Q and radius r on the relative stability of oxides and fluorides. Extracted from Baes Jr., C.F., 1974. Chemistry and thermodynamics of molten salt reactor fuels. J. Nucl. Mater. 51, 149–162.

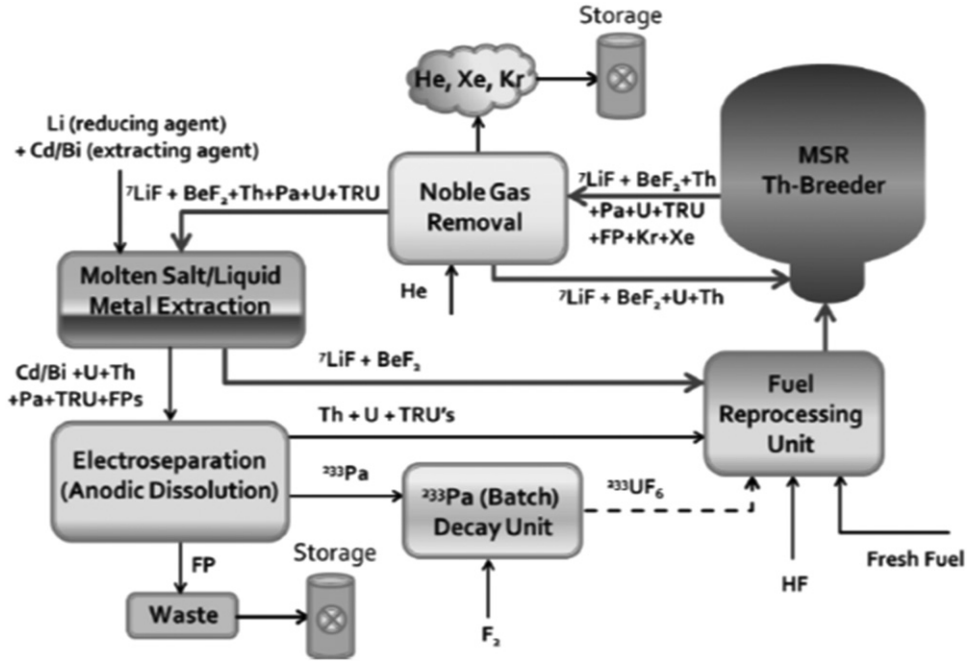

Fig. 5 Online fuel reprocessing scheme for MSBR spent fuel. Adopted from Uhlíř, J., 2007. Chemistry and Technology of Molten Salt Reactors – History and Perspectives. J. Nucl. Mater. 360 (1), 6–11.

from those compounds without significant neutron capture cross-sections – choosing corresponding oxides to convert corresponding fluorides does not change neutronics. Thus, for a system where the salt mixture consists of LiF, BeF_2, and ThF_4, the most advantageous reducing compounds narrow to Li_2O, BeO, and ThO_2; for LiF, BeF_2, ThF_4, and UF_4-based salt systems, the selective precipitants to convert PaF_2 include Li_2O, BeO, ThO_2, and UO_2. The solubility of metal oxides in FLiBe generally decreases with the square of the cation charge and by the inverse of the ionic radius, originally assessed by Baes, shown in Fig. 4.[31] This corresponds to a decrease in heats of reaction which reasonably correlates with Z^2/r (for the cation) for the reaction shown in Fig. 4.[31] From this assessment, BeO is fairly insoluble in FLiBe and dioxides of Th, Pa, U, and Pu are increasingly insoluble (in that order). Transition and post-transition metals also form some insoluble oxides, but their oxides are not as important because the corresponding fluorides they form are unstable.

Fig. 5 shows the basic chemical processing scheme proposed during MSBR, adopted from Ref. [75] As mentioned earlier, some fluorides are problematic from a neutronics, rather than from a corrosion viewpoint and chemical processing is needed to selectively and sequentially extract them online.

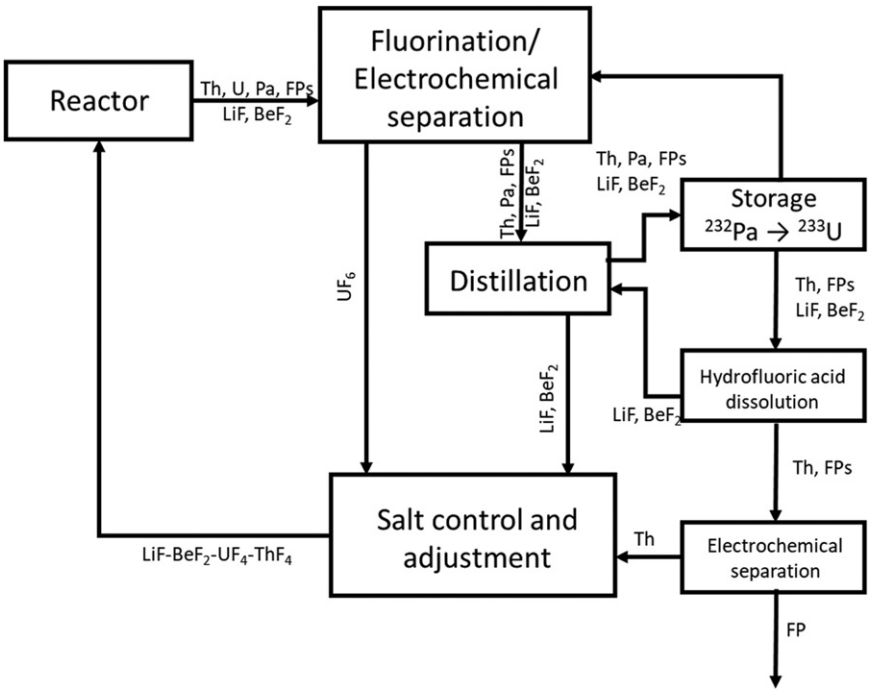

Fig. 6 Pyro-processing scheme for fuel salt reprocessing in China's TMSR-LF design. Adopted from Xue, H., 2015. Presentation: China's TMSR Programme. Oak Ridge National Laboratory.

In **Fig. 5**, spent fuel from MSBR was first sparged with He to bubble out noble fission gases like Xe and Kr at very high rates prior to storage since noble gases have low solubility in salt and do not form fluorides. The spent fuel then flows to a molten salt/liquid metal extraction unit in which everything in the salt phase is transferred to liquid bismuth. Li was proposed as a reducing agent, and Cd or Bi were proposed as extracting agents, each having their own recycle loops (omitted in **Fig. 5** for simplicity).[75] Clean salt is returned to the reactor and extracted species are forwarded to the electro-separation unit where ^{233}Pa, ^{233}U, and TRU are separated selectively and sequentially based on their redox potentials.[75] ^{233}Pa, which becomes fused into the salt as a fluoride compound, even in trace quantities in a neutron flux is unfavorable. ^{233}Pa is sent to a semi-batch decay unit for a duration of about 10 times the half-life of ^{233}Pa while it decays to ^{233}U. Then, ^{233}U is fluorinated with fluorine gas, which strips the ^{233}U in the form of $^{233}UF_6$ which is returned to the reactor in the form of UF_4.

Fluorination and electro-separation are still viable methods today to separate fission products, actinides and ^{233}Pa from fuel salt in China's developing Thorium Molten Salt Reactor (TMSR) program.[76–78] One of TMSR's key demonstrations are pyro-processing technology as shown in **Fig. 6**. This processing scheme relies on fluorination to recover U as UF_6 (a hexafluoride gas that dissolves to form UF_4 in FLiBe) and then electro-deposition of U-metal from FliBe–UF_4, with reported >92% recovery of U with this method.[76] Continuous online distillation can process up to ~6 kg/h of salt during reprocessing.[76] ^{233}Pa is extracted from distillation and stored away for several months. The TMSR 3-step strategy for the Th–U cycle is described elsewhere.[76] Tritium extraction methods (gas stripping, cryogenic separation), storage, and on-line coolant monitoring have been explored by the Chinese Academy of Sciences (CAS) and are the subject of several patents – i.e., Refs. 79,80.

4.09.4 Material Interactions With Molten Salt

Corrosion mitigation for nuclear materials in MSRs involves a concerted effort of initial salt purification, online salt purification, optimization of the reactor design and formulation of materials (compositions), and oftentimes, surface modifications of materials or coatings are necessary. This section will focus on corrosion, and the related irradiation effects issues of MSR graphite and metals will be touched upon in Section 4.09.4.2; a comprehensive guide to radiation effects in alloys and metals can be found elsewhere.[81] During MSRE/MSBR it was discovered that Hastelloy N suffered from pitting corrosion but also intergranular corrosion; intergranular cracking of all of the salt-facing alloy was discovered when surveillance specimens were strained at room temperature.[82–87] The Te-induced intergranular cracking of Hastelloy N was studied extensively at ORNL during the 1970s but also recently by China with their own Ni-base alloy GH3535.[87] GH3535 was developed for use in coolant loops, heat exchangers and piping for TMSR.[76,88] The formulation of GH3535 is described as similar to Hastelloy N, but it has been solution strengthened with 16 wt% Mo, 0.4–0.5 wt% Si stabilized Ni–Mo and primary precipitates in the alloys. Hastelloy N (Ni-16%, Mo-7%, Cr-5%, Fe-0.05%, C) is still a strong MSR candidate as a salt-facing alloy in FLiBe and FLiNaK. Type 316H

stainless steel is a high carbon formulation austenitic steel for high temperature service and a candidate container alloy along with Hastelloy N for FHR. 316H is ASME code-qualified in Section III, Division 5 up to 816°C and Hastelloy N is only code-qualified in Section VIII.[142] Extensive loop testing of Hastelloy N in early MSR programs at ORNL showed its maximum corrosion rate is below 5 μm/yr in the Li/Be/Th/U/F system,[44,82,85–87] less than 20 μm/yr in Li/Be/Zr/U/F and almost no corrosion in Li/Be/F coolant salt.[89] 316H corrosion in molten salt has not been fully considered in comparison. The performance of Ni-base alloys in MSRE/MSBR revealed He embrittlement.[90] Thus, a code-qualified type 316 stainless steel is also considered, although the Te-induced cracking phenomena will affect both metals.

The two major modes of salt compatibility testing of materials are static capsule (open or closed) and (low-flow or forced circulation) loop testing. In the low-flow or TCL, the flow is generated by the difference in density of the salt in the hot and cold sections of the loop configuration (e.g., 7 ft/min for $NaBF_4$–NaF between a hot section of 687°C maximum and a cold section of 438°C[85]). The forced circulation loops (FCL) relied on pumping mechanisms to create a faster salt flow velocity. During the 1950s through early 1970s, ORNL conducted hundreds of thousands of hours of loop tests,[26,85,87,91] out-of-pile static capsule material compatibility tests as well as in-pile capsule irradiations[30,44,63,92] during ARE and MSRE/MSBR.

4.09.4.1 Chemical Compatibility of Metallic Materials for Primary and Secondary Circuits

Corrosion of materials is one of the biggest challenges for MSRs. For any high-temperature application, corrosion of metallic container alloys is the primary concern. For liquid fuel reactors, mitigating corrosion of metals is much more challenging than avoiding corrosion in clean, non-fueled salt applications like FHR; thus, most of the focus of this section is on liquid-fuel systems. Unlike other chemical environments where metals form a dense, protective oxide layer, metal oxide solubility in molten salts precludes passivation. Thus, the corrosion rate of metals depends on thermal gradients, salt flow rates and interactions between dissimilar metals. Solid fuel reactors with "clean" (non-fuel) coolant are expected to have considerably less material compatibility issues as long-term MSR design hopefuls.

Cr is added to enhance the oxidation resistance of most high-temperature alloys, but among major alloying elements it tends to dissolve readily in molten fluoride salts. The process has been shown to be strongly temperature-dependent.[81,84–86,93,94] The idea is to limit Cr dissolution through optimizing formulations of metals and also by robust redox control of the salt. The choice of salt, as summarized in Section 4.09.2, should be based on those whose constituents are not easily reduced by structural metals, Ni, Cr, Fe, Mo, etc. and that can be near equilibrium with salt constituents around 1000K. Cr is the most active major alloying component based on examination of free energies of formation (ΔG_f), see **Table 3** and standard molar heats of formation (ΔH_f) in **Fig. 1**. Oxidative attack on these alloys will likely result in selective oxidation of Cr.[59,86,87] Thus, the choice of metallic alloy for MSRs is expected to largely influence Cr content in the salt. Stainless steels like 316L and 316H (Fe–Cr) have higher Cr content than Ni-base alloys developed for MSRs like Hastelloy N, so they are more susceptible to corrosion in molten fluorides.

Many potential fissile (UF_4-containing), fertile (ThF_4-containing) or combined mixtures of salts were proposed for MSBR, and material compatibility tests were conducted especially with Hastelloy N and other container materials[46] but the choice of secondary coolant was an open query. MSRE fuel salt mixture was ZrF_4-based, LiF–BeF_2–ZrF_4–UF_4 (65–29.1–5–0.9 mol%). ZrF_4-containing salts were utilized as the fuel salt and primary-circuit heat transfer fluid in the ARE, NaF–ZrF_4–UF_4 (50–46–4 mol%).[46] During the ARE years, there were early in-pile tests with NaF–ZrF_4–UF_4 fuel mixtures in Ni-based INCONEL (Alloy 600) containers. More than 100 static capsules were irradiated in neutron fluxes from 10^{11} to 10^{14} n/cm^2 s and by varying the fission power density from 80 to 8000 W/°C at temperature between 1500 and 1600°F (815.6 and 871.1°C)[30] for irradiation times from 300 to 800 h.[30] Three types of INCONEL in in-pile FCLs were operated with NaF–ZrF_4–UF_4 melts at fission power densities of 400–800 W/°C, between 1500 and 1600°F maximum temperature and for 235–475 h at full power.[30] Corrosion of INCONEL in these conditions was deemed similar to that of the out-of-pile tests with penetrations less than 3 mm.[30]

Fluoroborate salt NaF–$NaBF_4$ compatibility with metallic container alloys was researched during the MSRE/MSBR although it was only considered a back-up option to NaF–ZrF_4 and FLiBe, two forerunners that had better compatibility with Hastelloy N.[44,85] The interactions of trace amounts of oxides, air or moisture (either in the salt or cover gas) with fluoroborate salt correlate with the level of alloy corrosion,[92] which has been shown to be selective leaching of Cr from alloys through the following reactions:

$$H_2O + NaBF_4 \leftrightarrow NaBF_3OH + HF \tag{5}$$

$$NaBF_3OH \leftrightarrow NaBF_2O + HF \tag{6}$$

$$6HF + 6NaF + Cr \leftrightarrow 2Na_3CrF_6 + 3H_2 \tag{7}$$

Hydrolysis of the fluoroborate group (–BF_3) in the presence of moisture in the cover gas occurs rapidly, generating HF which is known to be corrosive to MSR metals and other reactor materials, Reaction (6). In fact, a previous Hastelloy N loop using equimolar NaF–ZrF_4 salt that was saturated with HF operated for only 200 h before loop operation had to cease due to becoming plugged with nickel corrosion product.[66] Some earlier works during MSBR conceptualization in the 1970s tend to show the potential for hydrogen- and oxygen-containing species, that resulted from hydrolysis of fluoroborates, to sequester tritium.[92] The discovery of proton-containing species $NaBF_3OH$ was the first evidence that these H isotopes could be stabilized in fluoroborate salt mixtures. BF_3OH^- ion was thermally stable in the presence of Hastelloy N, which could indicate that the species is stable under MSBR operating conditions.[92]

Extensive testing of $NaBF_4$–NaF (8–92 mol%) was conducted in a TCL constructed of Hastelloy N called NCL-20 between 1969 and 1972 for 19,930 h.[44,85] The specimens tested were 14 standard formulation Hastelloy N and two Ti-modified Hastelloy

N alloys. The hot section of the loop had a maximum temperature of 687°C and the cold section was air cooled to around 438°C to maintain a ΔT of about 249°C. Overall, the compatibility of $NaBF_4$–NaF was deemed good based on this extensive loop compatibility test.[44,85]

Hastelloy N compatibility with LiF–BeF_2–ZrF_4–UF_4–THF_4 (70–23–5–1–1 mol%) was extensively studied in TCLs after all the MSRE salt-facing alloy exhibited shallow intergranular cracking when strained at room temperature.[84–86] A loop was constructed mostly of Hastelloy N but also with Hastelloy N modified with 2% Nb (thought to reduce cracking at weldments) was operated for 9.2 yr between 560 and 700°C at ORNL.[86] Loop operation ended after a failure – a salt leak – in the hot section. The maximum corrosion rate of Hastelloy N was estimated to be about 0.04 mm/yr.[86] A large amount of Cr carbide depletion in the form of surface etching was observed via electron microprobe imaging. Attack and void formations, up to 3–4 mm deep into the matrix, were identified in the heated areas (675–695°C), while deposition was noted in the cooler areas at 580°C. Little surface change was noted up to 593°C in the midpoint region. Chemical analysis revealed a dramatic increase of Cr in the salt, compared to little or no change in the concentration of other elements. This finding corroborates previous studies,[59,95] as well as thermodynamic assessments.[96]

Subsequently, a TCL constructed of Hastelloy N was operated for 3.4 yr at a maximum temperature of about 704°C and a minimum temperature of about 538°C. Additions of 500 ppm FeF_2 were added to the loop to study the subsurface void formation/pitting of Hastelloy N.[87] It was concluded that the increase in CrF_2 was strongly correlated with the loss of Cr from Hastelloy N, especially in the loop hot section. The main sources of CrF_2 productions were likely from reactions of Hastelloy N with: (1) impurities like TF; (2) fuel constituents like (UF_3 and UF_4), and (3) from atom displacement reactions between FeF_2 and NiF_2 and Cr to form additional CrF_2.[86,87]

For the TMSR program, China has proposed Ni and CrN coating layers on GH3535 to mitigate corrosion attack by molten fluoride salts.[97] They have also researched Ni and CrN coatings on GH3535 alloy exposed to FLiNaK at 700°C for 100 h.[97] Uncoated, the alloy microstructure was impacted up to 49 μm in 100 h. The corrosion was less severe with GH3535 electroplated with Ni, but voiding at the interface and interdiffusion of Fe and Cr into the Ni plating resulted in degradation of the alloy and coating.[97] However, a CrN protective layer in between the Ni-plating and GH3535 showed significantly improved corrosion resistance due to forming a barrier to interdiffusion.

Te embrittlement has been studied recently in pure Fe, stainless steels, Hastelloy N and GH3535. A Te–Cs liquid metal embrittlement model would not consistently describe the embrittlement phenomena in stainless steels. In GH3535 the embrittlement is believed to be from nucleation of numerous intergranular surface cracks caused by Te penetration. Chromium tellurides were observed at both grain boundaries and intergranular carbide-matrix interfaces in the alloy when it was exposed to Te vapor. Intergranular tellurides were also confirmed recently by the work of Jiang.[97,98] The grain-size effect of Te embrittlement phenomena was studied for Hastelloy N, Type 316 stainless steel and GH3535.

McNabb concluded that the cracking frequency decreased, and the depth of cracking increased with grain size in Te-penetrated Hastelloy N.[99] Similar conclusions were reached for 316 stainless steel by Arima *et al.* when specimens were tested under different oxygen potential with Te vapor.[100] Thus, the advantage of fine-grained alloys in resisting Te diffusion and Te induced cracking have been realized. For GH3535, a cross-sectional image and chemical maps are provided in **Fig. 7** via scanning electron microscopy coupled with electron dispersive spectroscopy (SEM/EDS)[98] for specimens exposed to Te vapor in sealed quartz tubes. Cr depletion was typical where there was significant Te penetration at grain boundaries. The fine-grained GH3535 in this study clearly shows more outward growth but less Te penetration compared to a coarse-grained formulation. Overall, the fine-grained formulation of GH3535 exhibited thicker outward growth and the coarse grained, in contrast, formed continuous inward growth. The outer layer consisted mostly of Ni_3Te_2 and Cr_3Te_4 phases while the intermediate layers contained Ni_3Te_2 and M_6C-carbides, Fe-rich gamma phases and a little Cr_3Te_4 and MnTe.[98] In the residual matrix, Mo, Fe, Si, and C became greatly enriched. Coarse grained specimens had deeper subsurface Te penetration resulting in a large deterioration of tensile properties compared to fine-grained specimens.[98] **Fig. 8** shows the surface grain structure in polarized optical micrographs of 316H and Hastelloy N as well as SEM backscattered electron images, respectively. Polarized light is a contrast-enhancing tool in light microscopes that is useful for revealing grain structure and distinguishing what is optically isotropic (dark) or anisotropic (bright). Comparing **Fig. 8(C)** and **(D)**, Hastelloy N for MSR has fine carbide precipitates that help mitigate the Te-embrittlement issue.

4.09.4.1.1 Graphite for the reactor core

For purposes of corrosion evaluation, graphite is a synthetic material composed of nearly pure carbon; and its microstructure is comprised of filler grains of coke (from petroleum or coal, etc.) and binder (typically coal tar pitch). Gas evolution in graphite during the graphitization process creates porosity in graphite. For purposes of comprehending its radiation response and overall material performance in a nuclear reactor, one must also consider the highly complex structure of graphite and its peculiarities. The structural complexities include filler grain size and shape distributions, grain orientations, pore size and shape distributions, and a proportion of less-graphitic carbon binder.[101] Production of graphite usually happens on a large scale that is less amenable to nuances nor very detailed process control. Thus, there is batch to batch, block to block material variability and a degree of inhomogeneity in microstructure and properties even within a single block. Compared to the 1950s, today's production of multiton quantities of highly graphitized, high-purity, isotropic nuclear-grades of graphite has reached high maturity. Nuclear-grades of graphite conform to the rigors of chemical purity, coefficient of thermal expansion (CTE) isotropic ratios and bulk density as prescribed in ASTM D7219-08.[102] Fuel matrix graphitic materials are not included in these standard guidelines for nuclear-grade graphites. Because fuel matrix carbon materials are difficult to obtain commercially, data is not widely published. This type of carbon matrix is only partially graphitized. Graphitic fuel matrix carbon is fabricated with the fuel kernel so the graphitization

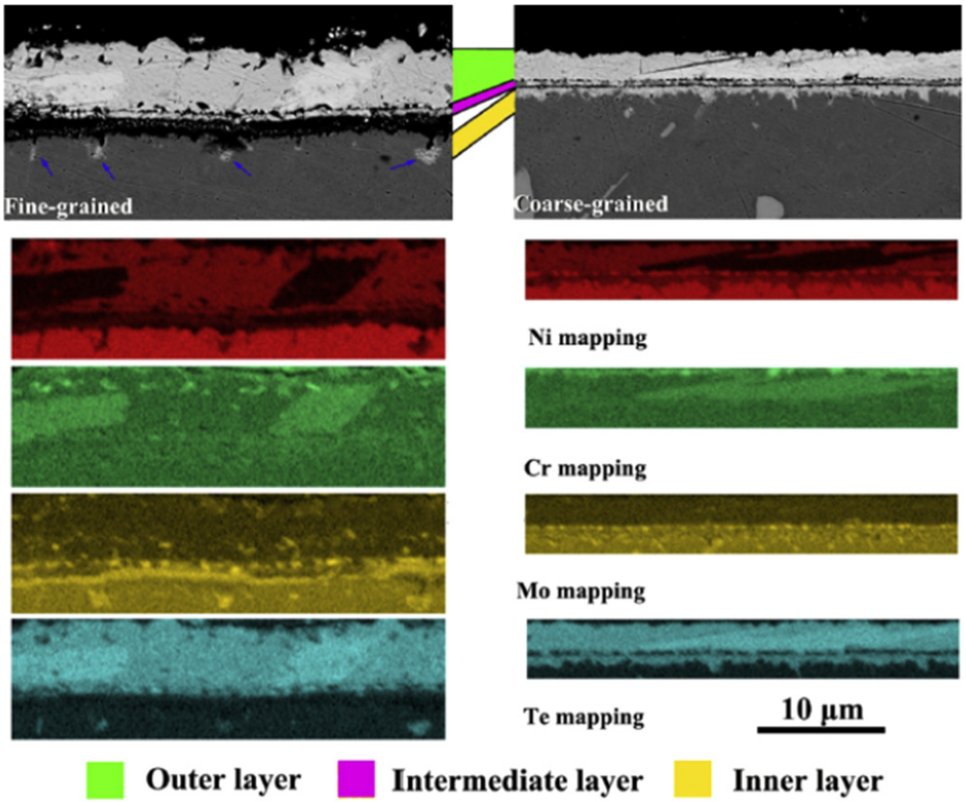

Fig. 7 Backscattered electron images and EDS mapping of fine (~46 μm) and coarse-grained (~107 μm) GH3535 after Te penetration experiments. Three different layers, outer, intermediate, and inner were observed in cross-sectional examination, as indicated. Extracted from Jiang, L., Fu, C.-T., Leng, B., *et al.*, 2019. Influence of grain size on tellurium corrosion behaviors of GH3535 alloy. Corros. Sci. 148, 110–122.

temperatures are around 1900°C compared to 2800–3000°C for fully graphitic material. **Fig. 9(A)** and **(B)** show SEM secondary electron micrographs of superfine grained (~20 μm) isotropic nuclear-grade graphite IG-110, **Fig. 9(C)** and **(D)** show medium-grained (<1.6 mm) nuclear-grade NBG-18 and graphitic matrix carbon in **Fig. 9(E)** and **(F)**. The grain sizes and internal textures are distinctly different; for instance, for **Fig. 9(C)** and **(D)**, NBG-18 has some large pores compared to the others and flakey carbonaceous sheets at high magnification. In **Fig. 9(E)** and **(F)**, the graphitic matrix by comparison has the finest grain size among the three grades, around 10 μm. In FHR, for instance, much of the pebble-bed core will be comprised of this graphitic matrix carbon.

Graphite has been used extensively as moderator, reflector and core structural material since the first reactor pile.[9] In thermal reactors, graphite is the moderator and reflector material but in fast reactors with an un-moderated core, graphite is typically only a reflector material. Graphite has favorable thermal, mechanical and neutronic properties, has low economic cost and can be easily machined. To a nuclear graphite expert, each grade of graphite is infinitely different, requiring extensive chemical and radiation testing of specimens from axial and transverse orientations of as-received material, a statistical sampling between batches of a billet and finite element modeling to describe its evolution in a neutron flux. Graphite is vital to the success of MSRs. Other than the salt, graphite is the material that will comprise most of the core volume. Graphite, in addition to resisting corrosion by molten salt, must also withstand neutron irradiation. Because of the large void volume of nuclear graphites, another concern is the potential for graphite to retain fission products (Xe, T, etc.) from salt and gas permeation; this issue could impact tritium distribution levels in MSRs and coolant chemistry control. Previous studies have reported that the impregnation of graphite with molten salt may change the coefficient of thermal expansion and accelerate the damage rate for graphite.[103,104]

Corrosion mechanisms can be accelerated by salt and gas permeation into graphite pores since pores significantly increase the accessible surface area for chemical interactions. The assumption in some earlier works that graphite does not corrode in molten salt is not true. These concerns, in addition to the salt permeation, potential tribological issues[105,106] and T uptake issues, form the basis for proposing seal coatings on graphite and lower porosity material by several researchers during MSRE but also recently by CAS.[104,107–112] The MSRE graphite grade was CBG; a material that would not be considered a nuclear grade according to today's standards. One of the trusted modern grades of graphite is IG-110, a superfine grained, isotropic, iso-statically molded grade produced by Toyo Tanso in Japan. It has about 18%–20% open porosity. It has a long operating history since the DRAGON HTGR in the UK. Researchers at CAS have recently tried to seal this graphite to mitigate the salt permeation issues.[107,109–114] In addition to sealing the surface of graphite, CAS has also tested He permeability (to test Xe permeability) in very low porosity grades of industrial graphites like POCO graphites AXF-5Q[114,115] and ZXF-5Q. **Fig. 10** shows an SEM secondary electron image of ZXF-5Q

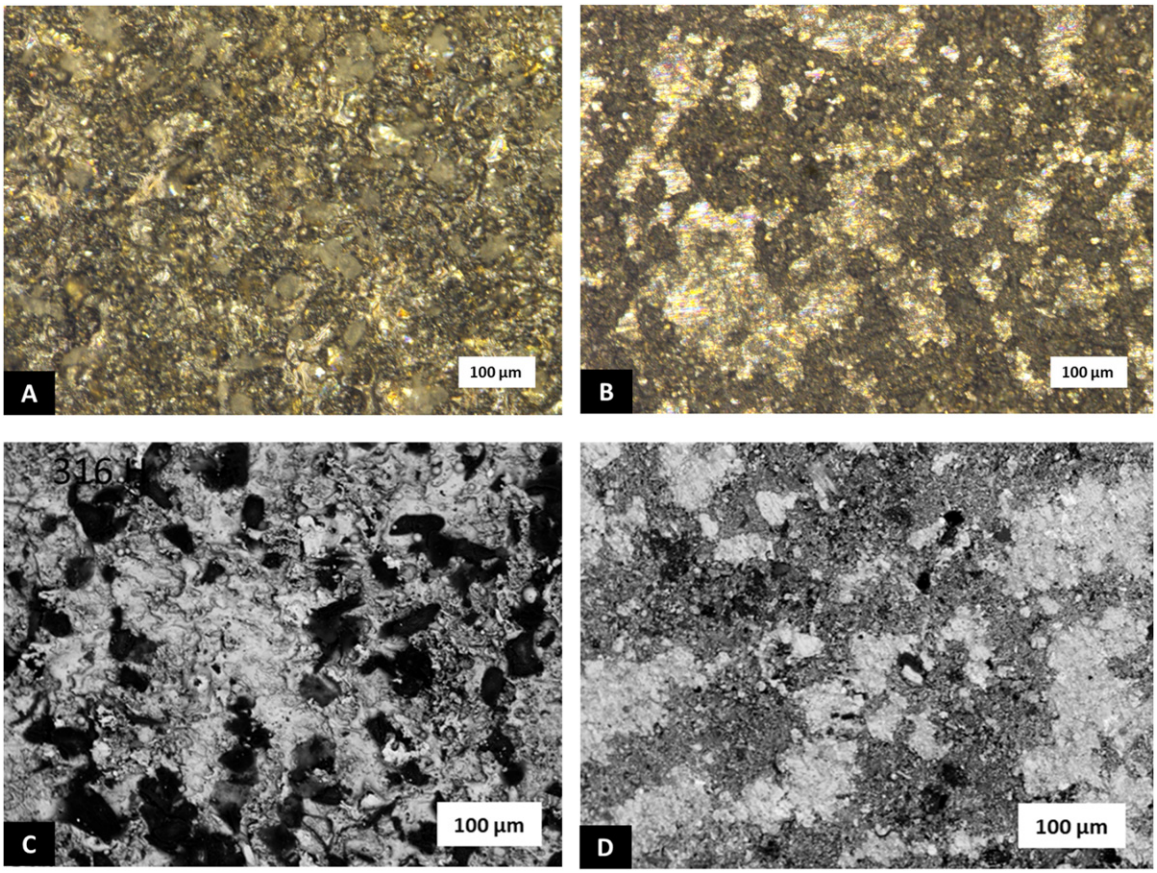

Fig. 8 Polarized optical micrographs of (A) Hastelloy N surface grain structure and (B) 316 H. Backscattered electron micrographs of (C) Hastelloy N and (D) 316 H microstructure.

with entrance pores around a few microns. China's TMSR program has also developed ultrafine grain nuclear graphite, NG-CT-50,[76] with nanopores to reduce salt permeation. Code-qualification of this grade for MSR use is underway.[76]

For liquid fuel systems where fissions are occurring in unclad fuel salt mixture, volatile fission products like Cs, Te, Rb, and I are expected to be driven by their own thermodynamic potentials. However, noble fission gases like Xe and Kr will likely have a high mobility through structural materials in MSRs.[11,116] Xe is a significant neutron poison (σ_{th} 2.6 billion barns). It was proposed during MSRE to strip Xe from fuel salt by purging with He.[93,117] Large amounts of Xe could contact graphite surfaces, and excessive retention (deemed $>0.5\%$ for a breeder reactor like MSBR) will result if the gas permeates the graphite surface.[93] If ^{135}Xe does not undergo neutron capture, it can decay into ^{135}Cs, a high-yield, long-lived isotope. Decay products of ^{135}Xe and ^{85}Kr – Rb, Cs, Sr, Ba, Ln, Zr – were discovered 1–2 mm into MSRE graphite.[93] Te, Mo, Ru and I were also 1–2 mm in graphite and Mo, Te, Ru, and Nb were plated out on MSRE graphite as fluoride compounds.[93]

Generally, the high surface tension of molten salts does not allow the salts to wet graphite. During MSRE, the molten fluoride salts at 700°C had a surface tension of about 230 dynes/cm (0.23 N/m) and a contact angle of 150° with graphite.[11] The surface tension is the pressure difference on both sides of the molten salt meniscus. The resistance of graphite to salt penetration is well-described by the Washburn relation in Eq. (8), which relates the graphite pore size and surface tension to capillary pressure of the infiltrating fluid into the pore,

$$\Delta p = -\frac{4\gamma \cos\theta}{\delta} \tag{8}$$

where δ is the entrance pore diameter of penetrated pores, Δp is the pressure difference, γ is the surface tension, and the θ is the contact angle.[11,118] Assuming the non-wetting characteristics of the molten fluoride salts are not altered, it was concluded that the pressure difference across accessible pores is controlling for liquid salt permeation up to 1 μm.[11] However, a reduction in the gas permeability of graphite will probably require the entrance diameters of accessible pores to be much less than 1 μm.[11]

Graphites of very low porosity were proposed at ORNL to address the issue of Xe diffusion into graphite during MSBR,[67] but the PyC sealing work was only a partial success. During the irradiation tests of PyC coated graphite, the PyC caused graphite swelling to occur at even lower fluences. Currently, seal coatings of PyC and SiC as well as resin impregnation methods on IG-110 have been proposed by researchers in China to solve the salt permeation issue. Based on these technologies, the task of coating and irradiating coated MSR graphite faces some notable challenges.

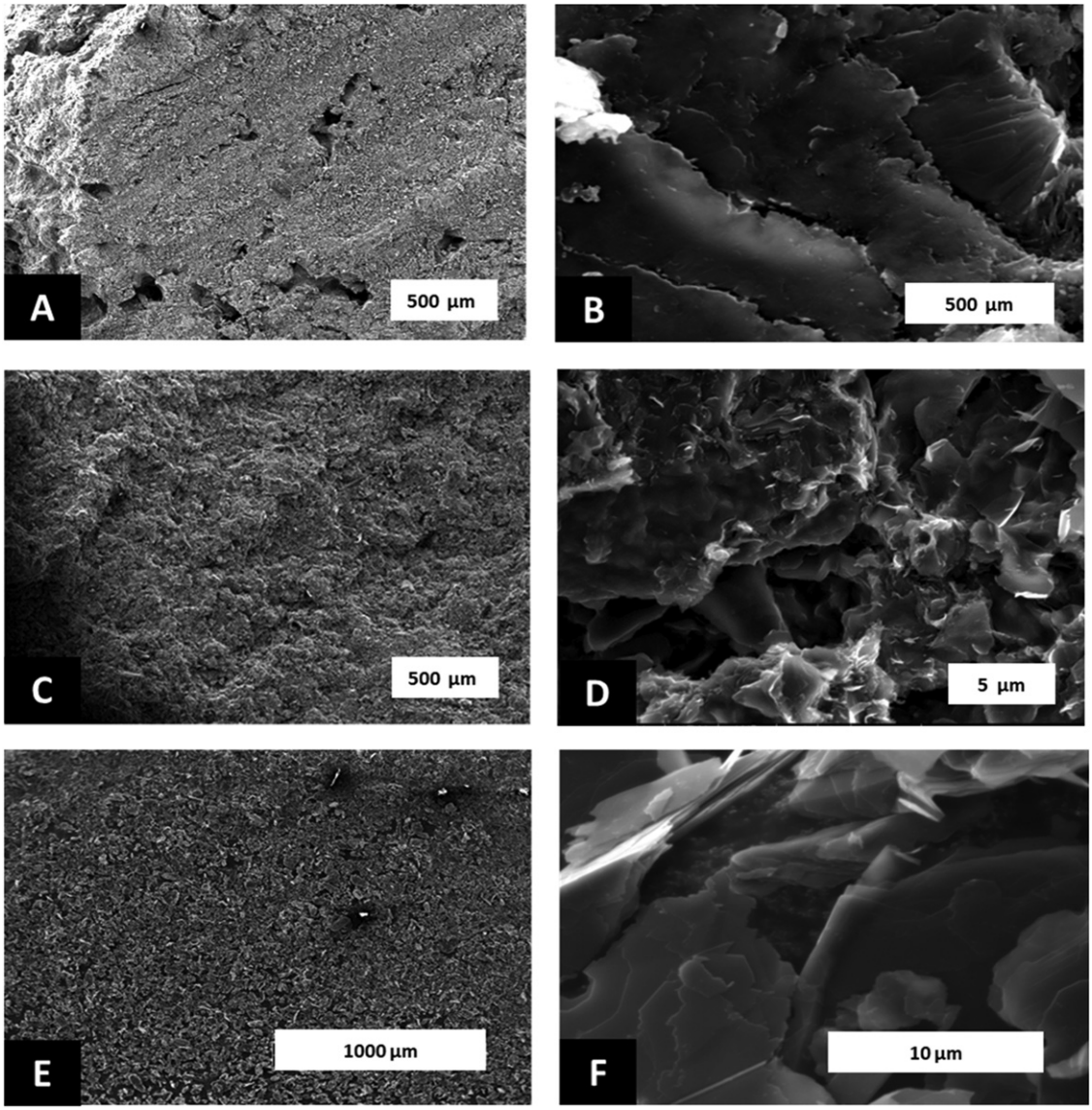

Fig. 9 Secondary electron images of various reactor grades of graphite: (A) and (B) NBG-18, (C) and (D) IG-110 and (E) and (F) graphitic matrix carbon.

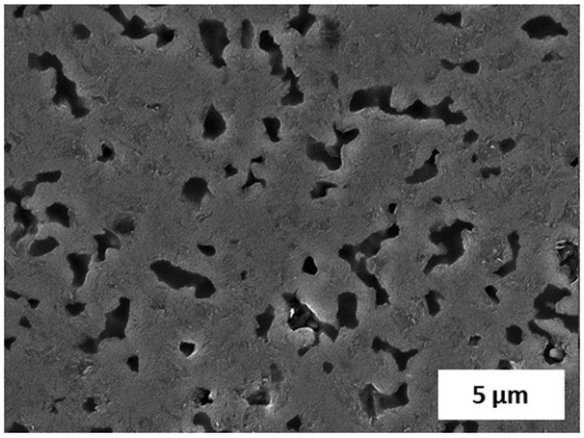

Fig. 10 Secondary electron image of the microstructure of ZXF-5Q, low porosity non-nuclear grade graphite.

Although some earlier works have reported that graphite does not corrode in molten fluoride salts, more recent studies have shown that graphite can cause a more aggressive corrosion and carbide depletion of metals in molten fluoride salts. Olson *et al.* observed more weight loss of Hastelloy N, Hastelloy X, Haynes Alloy 230, INCONEL 617 and Incoloy 800 H in FLiNaK at 850°C when tested in graphite containers, compared to metal containers.[94,119] Intense corrosion – more than reasonably expected – was observed on the salt-facing walls of the graphite crucibles. Chromium carbide phases were identified on the crucible interior walls. The metal coupons were corroded predominantly along the grain boundaries. Graphite is more electropositive than Cr, and Olson asserted that corrosion was initiated when graphite and alloys were in electrical contact. Thus, graphite has a better tendency to anodize and reduce Cr^{2+} to Cr^{3+} ions on its surface.

Zheng[120,121] tested 316 L in nuclear-grade graphite and stainless-steel lined crucibles and static corrosion tests were conducted at 700°C and the samples were examined after 1000, 2000 and 3000 h of testing. Microstructural characterization revealed intergranular corrosion and formation of $MoSi_2$ phase. The grain boundaries on the surface of the samples tested in graphite crucibles were corroded to a greater depth than those in stainless steel crucibles. The stainless steel tested in graphite also exhibited carbide phases of Mo_2C, Cr_7C_3, and Al_4C_3 in the form of nanometer sized particles due to C from graphite migrating to the stainless-steel surface. Considering Cr-depletion conditions at the surface, the subsurface was also affected by secondary phase formations, mostly at high-angle grain boundaries. The maximum corrosion rate of 316 L in these conditions was projected to be ~16 μm/yr in the absence of graphite (>20 μm in the presence of graphite).

More aggressive corrosion attack has been observed for stainless steel 316L as well as Hastelloy N in Zr-reduced FLiNaK by Sellers *et al.*[122] Non-nuclear grade AXF-5Q was added to stainless steel 316L crucibles with Hastelloy N and stainless steel 316 L coupons at 850°C for 1000 h. Some of the static tests included graphite samples. In the crucibles with graphite samples, the Hastelloy N and stainless steel 316L exhibited distinct corrosion behavior. The accelerated corrosion of 316L in the presence of graphite resulted in twice as much weight loss and void formation). Hastelloy N gained weight and became plated with a layer rich in Fe and Cr.

4.09.4.1.2 Ceramic composites in advanced MSRs

Ceramic matrix composites (CMCs) have wide applicability in many fields including turbine hot section components and high temperature aerospace applications. The choice of fiber and the fracture toughness are widely studied, but the corrosion behavior in molten fluoride salts has only been studied recently. The CMC candidates are intended for areas of higher neutron fluxes, such as control rod liners and guide channels, core barrel, core support structures and other core internals of FHR.[16] Both SiC fiber re-enforced SiC matrix composites (SiC_f/SiC) and carbon fiber re-enforced carbon (or graphite) matrix composites (C_f/C) have been proposed as FHR candidate CMCs. C_f/C composites are known for their high tensile strength.[123] Compared to SiC_f/SiC composites, C_f/C composites have a more established market and maturity as a commercial material having many available options on the market from ordinary to special architectures. One clear disadvantage compared to SiC_f/SiC composites is that C_f/C composites are far more susceptible to gradual dimensional change and radiation anisotropy.[124] Their corrosion behavior is not well-studied for MSRs, but it is reasonably expected to exhibit a similar corrosion behavior, salt permeation behavior and radiation response as other C-based materials like graphite. Currently, the molten salt corrosion behavior of C_f/C composites are a technical gap.

Fig. 11 shows an electron micrograph of the SiC fiber architecture of a SiC_f/SiC composite and an optical image of a corrosion coupon of the same material. Monolithic SiC is brittle by nature, thus necessitating a composite structure. For SiC_f/SiC composites, the fibers provide additional strength, reliability and performance predictability. The composites typically have some thickness of CVD SiC overlayer. One drawback of a composite structure is the reduced gas tightness. SiC has been an integral layer of TRISO fuel developed in the 1960s for HTGRs. Yajima *et al.* in the 1970s developed the continuous SiC-based fiber and soon after SiC_f/SiC were being developed

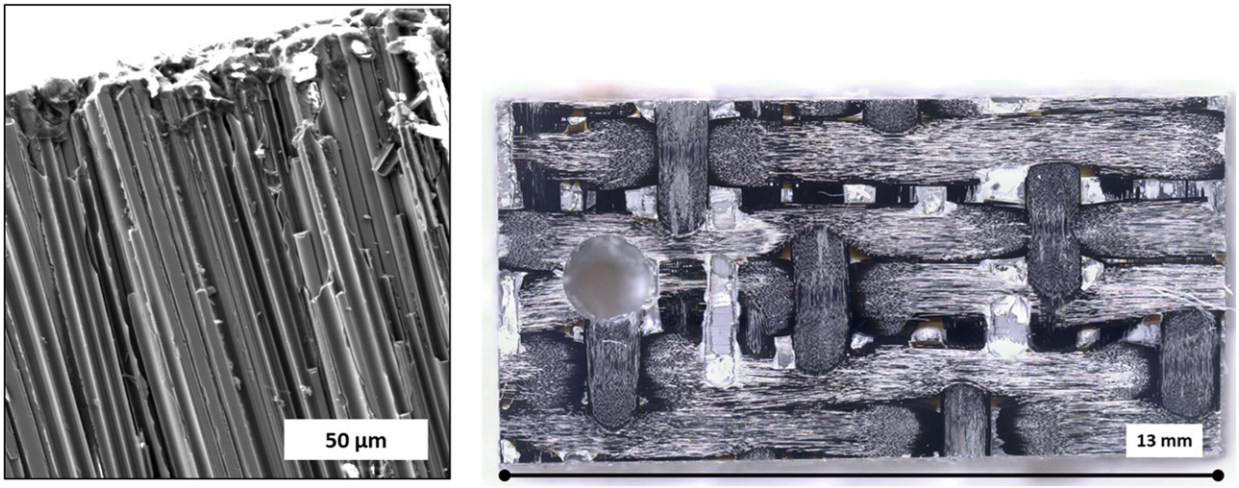

Fig. 11 Secondary electron image of exposed fiber region (left) of silica polished Rolls Royce® CVI SiC_f/SiC composite with 2D satin weave SA3 fiber reinforcement and (right) a coupon for corrosion testing.

by several processes including: chemical vapor infiltration (CVI), liquid silicon infiltration (LSI) or melt infiltration (MI), polymer impregnation and pyrolysis (PIP), and transient eutectic phase (TEP) processes.[125] Demonstration of the first radiation-tolerant SiC_f/SiC composite occurred around 1999 with third-generation near-stoichiometric SiC fiber composites for the US-Japan fusion materials collaboration project[125]; today, the manufacturing processes have reached high maturity. In future advanced FHR designs, SiC_f/SiC composites could be an attractive option for shutdown rod guide channels, which would eliminate the need for a central graphite reflector in an annular core.[16] SiC seal coatings on graphite have also been proposed by CAS.[108,118]

The general radiation tolerance of third-generation SiC fiber composites has been demonstrated through the CVI process and the nano-infiltration and transient eutectic-phase (NITE) process over a broad range of irradiation conditions, 300–1300°C and >70 dpa fluence, with some variations in the limitations of radiation resistance for specific materials.[125] Composite radiation stability, for a long time, was the primary technical feasibility factor and focus in early phases of SiC_f/SiC composite study for fusion applications.[121] At first, the composite radiation stability was only in the purview of fusion applications, but now significant activities are pursued with SiC_f/SiC in fusion and fission technologies. A significant effort has been undertaken to understand fundamental radiation damage processes (irradiation creep, conductivity change, etc.) and environmental effects on the material in pursuit of ASME code qualification. For instance, stability of NITE SiC_f/SiC composites have been demonstrated under neutron irradiation up to intermediate fluence levels.[126] High dose irradiation effects have been studied with CVI SiC matrix composites with PyC/SiC multilayered interface irradiated up to 71–74 dpa at 300, 500, and 800°C at the ORNL High Flux Isotope Reactor (HFIR).[127] However, a detailed undertaking of the fundamental radiation processes of these composites are beyond the scope of this article; some of the main literature references for developments of SiC_f/SiC composites for nuclear applications are provided by.[125,128–130] One clear literature gap for SiC_f/SiC in MSRs is the lack of SiC irradiations in molten salts to fully comprehend its corrosion and radiation behavior in MSRs.

As opposed to air or steam environments, SiC does not form a protective oxide layer in molten fluoride salts.[131–133] Its corrosion has been studied mostly in FLiNaK used as a surrogate in sealed capsule tests by CAS and other institutions. SiC and FLiBe corrosion has been studied but there is less corrosion data in FLiBe for all materials in comparison. CAS tested SiC and SiC_f/SiC in molten FLiNaK around 700°C. These studies have tested SiC in purified FLiNaK, the effect of added Cr^{3+} impurity on SiC corrosion in FLiNaK,[131,134] the effect of intrinsic oxygen in SiC materials,[132] as well SiC composite corrosion.[135,136]

Si in SiC has been shown to preferentially dissolve into FLiNaK via a surface etching mechanism where SiF_4 goes into the salt and a C-rich overlayer remains on SiC with chromium carbides. The generalized reaction is shown in Reaction (9).

$$Si^{4+} + 4F^{-} \rightarrow SiF_4 \tag{9}$$

Thermodynamic data suggest that chromium carbides will be favored over other major alloying elements in molten FLiNaK.[137,138] These reactions were shown to accelerate with added impurities of CrF_2.[139] Overall, the corrosion behavior of SiC seemed favorable in purified FLiNaK tests around 700°C with minimal weight change from Si-loss among similar capsule experiments.[134] For the SiC_f/SiC, Yang[132] and Wang[135,136] showed preferential corrosion of the SiC matrix compared to the fibers of the composite in molten FLiNaK at 700°C, due to the slightly higher oxygen content of this matrix phase, as shown in **Fig. 12**. SEM micrographs showed exfoliation of the composite surface.

4.09.4.2 Radiation Effects on Material Performance in Molten Salt

Metallic alloy and graphite irradiation behavior was researched as early as the first MSRs. CMCs were proposed much more recently, typically in recent FHR designs. Along with chemical compatibility, materials must also exhibit radiation tolerance, and reactor design is influenced by these limits. The major radiation effects of materials from early MSRs are discussed here to enrich understanding of materials performance, particularly corrosion-related mechanisms in a radiation field. The advanced radiation mechanisms and models are best explained elsewhere and are beyond the scope of this article.

4.09.4.2.1 Radiation hardening and creep deformation in MSR metals

For MSRE, the annual corrosion depth of Hastelloy N was less than 5 μm/yr but two other problems were discovered after examination of in-pile surveillance specimens: radiation hardening due to accumulation of He at grain boundaries and the discovery of Te-induced cracking (stress corrosion cracking) on the inside surface of Hastelloy N piping after the metal was recovered after shutdown. Despite low dose, some Ni transmuted via a two-step thermal transmutation with delayed neutrons producing He[90]:

$$^{58}Ni + {}^{1}_{0}n \rightarrow {}^{59}Ni \tag{10}$$

$$^{59}Ni + {}^{1}_{0}n \rightarrow {}^{4}_{2}He + {}^{56}Fe \tag{11}$$

For the first issue, it was later discovered that carbide precipitates that normally occur in Hastelloy N could be modified to resist He embrittlement by providing trapping sites for He and preventing its migration to grain boundaries. For instance, the formulation of Hastelloy N with 2% Ti added to substitute for Mo (12%) and Si (0.1%) would form a fine carbide precipitate with good resistance to He embrittlement. For the second issue, Te is a fission product that interacted with metal to form tellurides, brittle intermetallic compounds at grain boundaries as discussed in Section 4.09.4.1. Numerous parts of the MSRE were examined, and all of the salt-facing metal exhibited shallow intergranular cracking in tensile testing at room temperature.[90] Although the Te flux was fairly low for MSRE ($\sim 10^9$ atoms Te/cm^2 s), cracks as long as 0.33 mm were discovered.

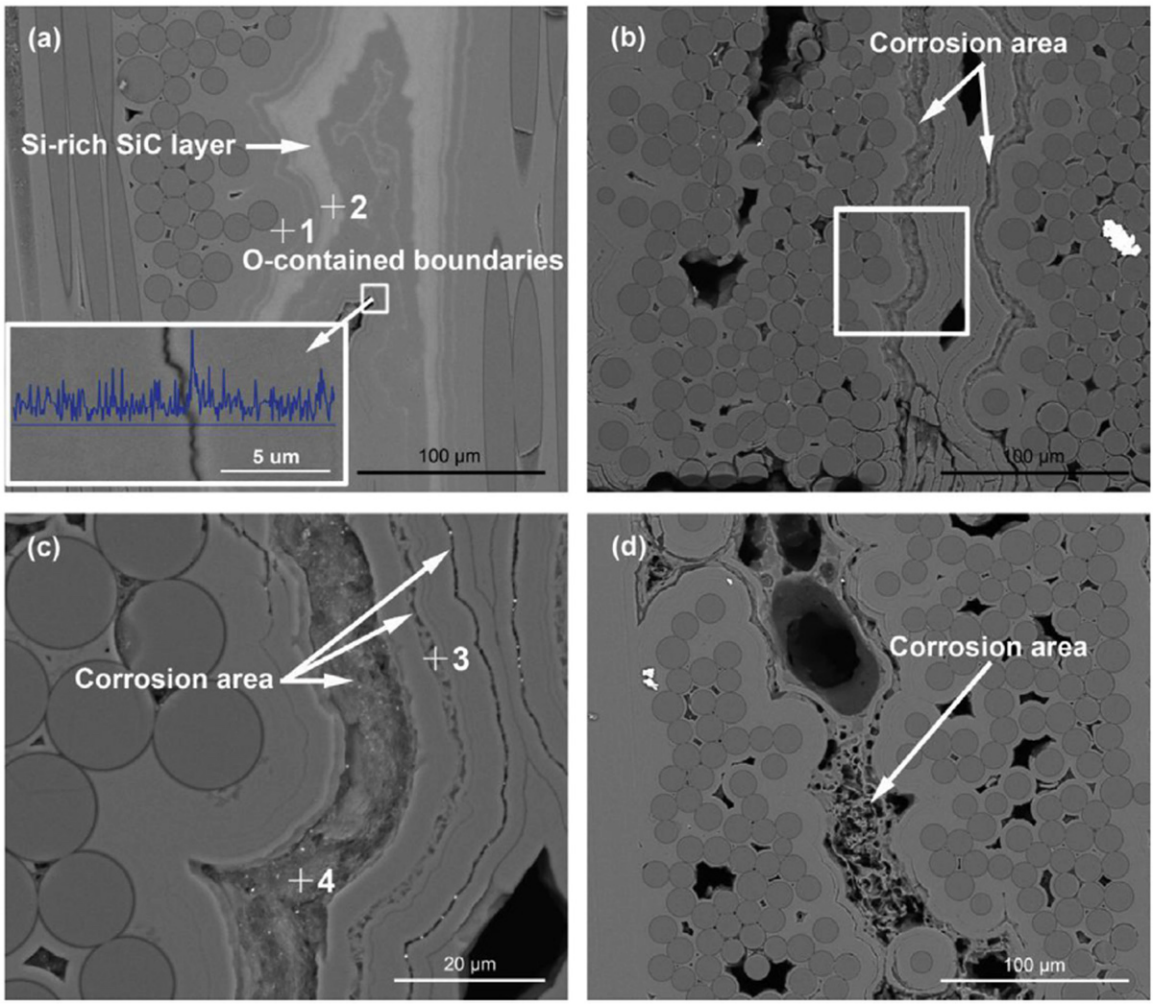

Fig. 12 Corrosion of exposed matrix regions around fiber bundles of SiC_f/SiC composite in FLiNaK at 700°C. Extracted from Wang, H., Feng, Q., Wang, Z., *et al.*, 2017. The corrosion behavior of CVI SiC matrix in SiCf/SiC composites under molten fluoride salt environment. J. Nucl. Mater. 487, 43–49.

Creep is the temperature and time dependent accumulation of inelastic (irrecoverable) strain leading to material damage and is a significant concern for materials operating under loads. Thus, creep deformation data is needed for materials to predict their service life. For MSRs, the operating temperature is around 700°C. Creep testing data of GH3535 between 650 and 750°C between 85 and 380 MPa were used to estimate the long-term creep strain and rupture life in MSR operating temperatures by CAS.[140] Material failure during creep was due to large strain localization accumulating at grain boundaries and triple points due to grain boundary sliding that results in cavitation, and microcracking led to large intergranular corrosion regions.[140] The effect of coarse grain boundary precipitates was not apparent in correlation with precipitate size when analyzing creep ductility. Large grain boundary precipitates can adversely affect ductility and rupture strain in Ni and Fe-base alloys during creep because these precipitates act as cavitation sites and enhance intergranular corrosion.

4.09.4.2.2 Graphite radiation behavior in MSRs

The life of the graphite is the life of the reactor. There could be a need to develop new MSR graphites based on current research and developments. One objective of the TMSR program in China is code qualification of NG-CT-50, a low porosity MSR-suitable graphite with entrance pores <1 μm. Recall, the MSRE moderator graphite was only envisioned to last about 4 years.[117] Irradiation-induced dimensional and property changes, which are functions of irradiation fluence, temperature and load, have strong implications on graphite component life that must be considered by designers and operators. Most material component lifetime assessments rely on finite element analysis, corrosion data and empirical data from material test reactor programs; this is no different for graphite. In terms of radiation effects, the main properties of concern are Young's modulus, strength, CTE and irradiation creep. For instance, if seal coatings are proposed for graphites, then the change in CTE of the coated system in a radiation field is obviously a parallel concern.

Because significant dimensional change and property change of graphite were observed in MSBR conditions of interest, research (for a time) was conducted on graphite behavior in MSRs to determine the most suitable grade of graphite, irradiation exposure conditions, effects on core power density, MSBR performance, graphite lifetime and replacement costs. For fast neutron fluences, the maximum permissible limit was determined to be $<3\times10^{22}$ n/cm^2 ($E_n >$ keV) at an effective temperature of 700°C with peak power density around 100 kW/°C for 2.5 years of reactor operation[11]; this was the permissible limit that would allow graphite to return back to its original volume. Simply, the radiation response of MSRE graphite was not suitable according to today's standards. Research at the time showed that isotropic graphites with large crystallites (less binder material) were needed. Older HTGR graphites like Magnox Pile Grade A (PGA), which was used as moderators in UK's first-generation gas reactors, are highly anisotropic because of the manufacturing process and raw material feedstock at the time[141]; anisotropic graphites are not suitable as moderator materials. Nevertheless, much stronger analogy for the graphite radiation response in MSRs is made to its response in past and operating graphite moderated, gas-cooled reactors, rather than direct results of MSRE graphite irradiations.

Today, much of the irradiation data and experience obtained in the gas-cooled reactor programs that focus on UK's Advanced Gas-cooled Reactor (AGR), VHTR programs, Japan's THTR, China's HTR-10 programs, etc. are applicable to MSRs, since those reactors also have a graphite-moderated core; pebble-bed gas reactors and FHRs will use the same ceramic fuel. With rising costs of decommissioning and longer lifetime extensions for power plants, the future generation reactors that use graphite like VHTRs expect replacement after 25–30 years of service life; for instance, a fleet of small modular reactors can provide flexibility for core replacement of one reactor unit while the others in the fleet continue producing power, reducing shutdown times. In the UK, many of the current generation graphite moderated reactors now producing power are operating beyond their design life. There is a need to extend the current graphite irradiation databases for higher temperatures and higher fluences to support these power stations.[141]

Other than use as a reflector material, there are not many institutions attempting to put graphite in a fast neutron flux for any other purpose. The large majority of developing MSR concepts are non-moderated fast breeder reactors that benefit from skipping the salt-reprocessing challenges for thermal liquid fuel reactors and skipping the moderator graphite salt permeation issues, see Section 4.09.4.1.1. During MSRE, 10%–30% of "noble metal" fission products deposition on graphite was discovered.[11] Assuming replacement of core graphite every 2 years, a reduction in the MSBR breeding ratio (~1.06:1) would be reduced by ~0.002 (~0.004 if replaced in 4 years).[11] It was also determined that sealing the moderator graphite with PyC reduced the Xe diffusivity to 10^{-8} ft^2/h (~10^{-5} cm^2/h) in addition to gas stripping that would keep Xe poisoning fractions around ~0.5%[11]; however, the PyC seal coating was only a partial success because of the unfavorable radiation response of the coated system (see Section 4.09.4.1.1). Based on these factors and irradiation tests of small graphite specimens, it was determined that graphite would be feasible for MSBR use, but efforts to develop improved graphites continued to be documented at ORNL until the point where the MSBR program was terminated. For advanced MSRs, many of the same issues identified with prior graphite use in MSRs still apply: choice of graphite and exposure conditions, radiation behavior, salt and gas penetration of graphite (including Xe permeability, T chemisorption, etc.), deposition of fission products on graphite (in liquid fuel designs), the effects of gas stripping, effect of fission products deposition and dimensional change on fuel performance.

Neutron irradiation causes individual crystallites in graphite to swell along the c-axis and shrink along the a-axis, increasing the distance between the graphene sheets resulting in anisotropic crystallite growth. Over time, shrinkage occurs due to closing of initial voids, and thermal stresses are generated. Most of the stress is relieved by radiation creep (inelastic strain); microcracks try to accommodate the internal shearing strains without causing gross volume growth. Once original microcracks close, they can no

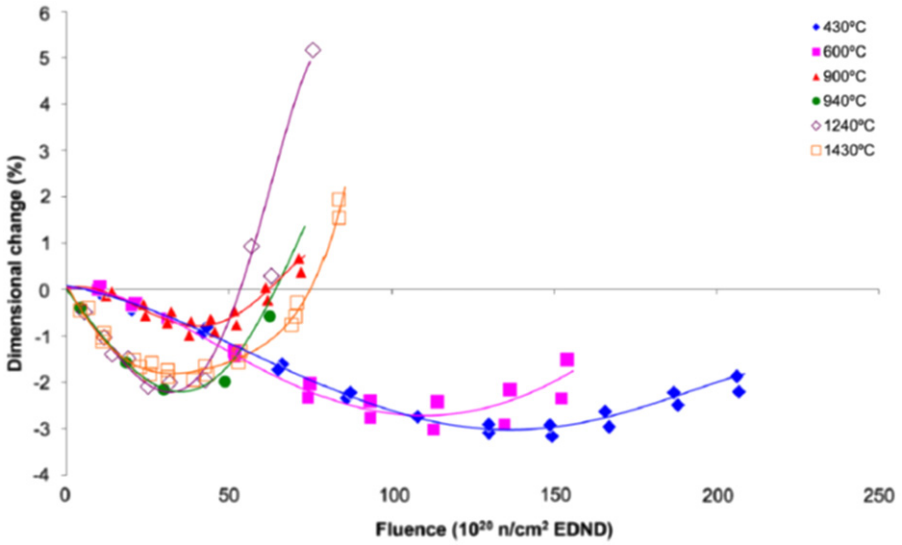

Fig. 13 Turnaround in neutron irradiated Gilsocarbon grade graphite. Extracted from Marsden, B.J., Haverty, M., Bodel, W., *et al.*, 2016. Dimensional change, irradiation creep and thermal/mechanical property changes in nuclear graphite. Int. Mater. Rev. 61 (3), 155–182.

longer accommodate internal strains from particle deformation and the internal strain is then accommodated by cracking (usually of the binder material). Within the tested temperature range, Fig. 13 shows the higher the temperature, the sooner the "turn-around" (transition from shrinking to swelling). The radiation response of Gilsocarbon grade graphite used in 14 of UK's current generation graphite reactors is referenced, because the grade has a long operational history and the data is readily available.[141] Fig. 13 shows linear dimension change data from 430 to 1430°C for irradiated AGR (Advanced Graphite Reactor) Gilsocarbon graphite samples. This radiation response is typical for most semi-isotropic, medium and fine-grained nuclear-grade graphites, but the response of one graphite grade should not be extrapolated to another.

The magnitude of internal stresses depends on fast neutron flux distributions and also on radiation creep. Graphite undergoes inelastic strain during neutron irradiation under stress at a temperature where thermal creep is considered negligible.[141] The stress–strain relationship for graphite is non-linear and a permanent set can be produced even at very low stresses. Because of the significance of irradiation induced creep to stress levels in graphite core components, robust creep models (especially to resolve the high dose and high temperature tensile creep data) have long been sought. As graphite ages in a service environment, it forms cracks; micro and nano-cracks have been discovered in present UK gas reactors. Cracks can eventually allow ingress of molten salt in MSRs.

Acknowledgment

The submission is being written by the author acting in her own independent capacity and not on the behalf of UT-Battelle, LLC, or its affiliates or successors, nor is she acting on behalf of any government agency.

See also: 4.01 Principles of Corrosion in Nuclear Systems: Theory and Analytical Methods. 4.02 Water Chemistry Control in LWRs. 4.15 Steam Oxidation in Accident Conditions. 5.18 Molten Salt Reactor Fuel and Coolant

References

1. Lane, J.A., MacPherson, H.G., Maslan, F., 1958. Fluid Fuel Reactors. Addison-Wesley.
2. Nunes, V.M.B., Queirós, C.S., Lourenço, M.J.V., Santos, F.J.V., Nieto de Castro, C.A., 2016. Molten salts as engineering fluids – A review. Appl. Energy 183, 603–611.
3. Nickel, K.G., 2010. Chapter 1.26. High temperature corrosion of ceramic and refractory materials. In: Quirmbach, P., Potschke, J. (Eds.), High Temperature Materials. Elsevier.
4. Rosenthal, M.W., Kasten, P.R., Briggs, R.B., 1970. Molten-salt reactors – History, status, and potential. Nucl. Appl. Technol. 8 (2), 107–117.
5. MacPherson, H.G., 1985. The molten salt reactor adventure. Nucl. Sci. Eng. 90, 374–380.
6. Hurst, C., 2015. Fuel for Thought: The Importance of Thorium to China. Available at: http://www.ensec.org/index.php?option=com_content&id=568:fuel-for-thought-the-importance-of-thorium-to-china&Itemid=395.
7. Vijayan, P.K., Basak, A., Dulera, I.V., *et al.*, 2015. Conceptual design of Indian molten salt breeder reactor. Pramana 85 (3), 539–554.
8. Staatz, M.H., Armbrustmacher, T.J., Olson, J.C., *et al.*, 1979. Principal thorium resources in the United States. In Geological Survey Circular 805. U.S. Department of Energy.
9. Kasten, P.R., 1964. The MOSEL reactor concept. In: Proceedings of the Third International Conference on the Peaceful Uses of Atomic Energy, Geneva. A Conf. 28/P/538.
10. Grimes, W.R., 1970. Molten-salt reactor chemistry. Nucl. Appl. Technol. 8, 137–155.
11. Kasten, P.R., Bettis, E.S., Cook, W.H., *et al.*, 1969. Graphite behavior and its effects on MSBR performance. Nucl. Eng. Des. 9, 157–195.
12. Cardarelli, F., 2000. Materials Handbook: A Concise Desktop Reference. Springer-Verlag.
13. Ghosh, S., Prabhakara Reddy, B., Nagarajan, K., Hari Kumar, K.C., 2014. Experimental investigations and thermodynamic modelling of KCl–LiCl–UCl_3 system. Calphad 45, 11–26.
14. Rao, C.J., Ningshen, S., Mallika, C., Mudali, U.K., 2018. Molten salt corrosion behavior of structural materials in LiCl-KCl-UCl3 by thermogravimetric study. J. Nucl. Mater. 501, 189–199.
15. Scarlat, R.O., Laufer, M.R., Blandford, E.D., *et al.*, 2014. Design and licensing strategies for the fluoride-salt-cooled, high-temperature reactor (FHR) technology. Prog. Nucl. Energy 77, 406–420.
16. FHR, , 2013. Fluoride-salt-cooled, high-temperature reactor (FHR) subsystems definition, functional requirement definition, and licensing basis event (LBE) identification white paper. In Integrated Research Project Workshop 1. FHR.
17. FHR, , 2014. Technical Description of the "Mark 1" Pebble-Bed Fluoride-Salt-Cooled High-Temperature Reactor (PB-FHR) Power Plant. UCBTH-14-002. FHR.
18. Flanagan, G.F., Holcomb, D.E., Cetiner, S.M., 2012. FHR Generic Design Criteria. ORNL/TM-2012/226.
19. E.N. Society, 2018. Table: Nuclear Reactors, World-Wide, Reactor Types. Available at: https://www.euronuclear.org/info/encyclopedia/n/npp-reactor-types.htm.
20. Brian, A., Andrew, W., Jeffrey, P., *et al.*, 2013. Safety and Regulatory Issues of the Thorium Fuel Cycle. NUREG/CR-7176. ORNL TM-2013/543. ORNL.
21. Fukuda, S., 2013. Flibe-tritium research for fission or fusion reactors at Kyushu University. J. Plasma Fusion Res. Ser. 10.
22. Scarlat, R.O., Peterson, P.F., 2014. The current status of fluoride salt cooled high temperature reactor (FHR) technology and its overlap with HIF target chamber concepts. Nucl. Instrum. Methods Phys. Res. Sec. A: Accel. Spectrom. Detect. Assoc. Equip. 733, 57–64.
23. Petti, D.A., Smolik, G.R., Simpson, M.F., *et al.*, 2006. JUPITER-II molten salt flibe research: An update on tritium, mobilization and redox chemistry experiments. Fusion Eng. Des. 81 (8–14), 1439–1449.
24. Morley, N.B., Abdou, M.A., Anderson, M., *et al.*, 2006. Overview of fusion nuclear technology in the US. Fusion Eng. Des. 81 (1–7), 33–43.
25. Ambrosek, J., Anderson, M., Sridharan, K., Allen, T., 2017. Current status of knowledge of the fluoride salt (FLiNaK) heat transfer. Nucl. Technol. 165 (2), 166–173.
26. Wilson, D., 2006. Assessment of Candidate Molten Salt Coolants for the NGNP/NHI Heat Transfer Loop. ORNL/TM-2006/69.
27. Wilson, D., Toth, L.M., Clarno, K.T., 2006. Assessment of Candidate Molten Salt Coolants for the Advanced High-Temperature Reactor (AHTR). ORNL/TM-2006/12.
28. Forsberg, C.W., Peterson, P.F., Williams, D.F., 2005. Practical aspects of liquid-salt-cooled fast-neutron reactors. In: Proceedings of the ICAPP'05, Seoul, Korea, May 15–19, 2005, paper 5643.
29. Stempien, J.D., Ballinger, R.G., Forsberg, C.W., 2016. An integrated model of tritium transport and corrosion in fluoride salt-cooled high-temperature reactors (FHRs) – Part I: Theory and benchmarking. Nucl. Eng. Des. 310, 258–272.
30. Grimes, W.R., 1967. Chemical Research and Development for Molten-Salt Breeder Reactors. ORNL-TM-1853.
31. Baes Jr., C.F., 1974. Chemistry and thermodynamics of molten salt reactor fuels. J. Nucl. Mater. 51, 149–162.
32. Reed, T.B., 1971. Free Energy of Formation of Binary Compounds. Cambridge, MA: MIT Press.

33. Stull, D.R., Prophet, H., 1971. JANAF Thermochemical Tables. NSRDS-NBS 37. U.S. Department of Commerce, National Bureau of Standards.
34. Bamberger, C.E., Ross, R.G., Baes, J.C.F., 1971. The oxide chemistry of plutonium in molten fluorides and the free energy of formation of PuF_2 and PuF_4. J. Inorg. Nucl. Chem. 33, 767–776.
35. Beneš, O., Konings, R.J.M., 2013. Thermodynamic assessment of the LiF–CeF_3–ThF_4 system: Prediction of PuF_3 concentration in a molten salt reactor fuel. J. Nucl. Mater. 435 (1–3), 164–171.
36. Thoma, R.E., 1959. Phase Diagrams of Nuclear Reactor Materials. ORNL-2548.
37. Barton, C.J., Stehlow, R.A., 1961. J. Inorg. Nucl. Chem. 18, 143.
38. Renault, C., *et al.*, 2009. European molten salt reactor. In: Proceedings of the Seventh European Commission Conference on Euroatom Research and Training in Reactor Systems, Prague, Czech Republic, Jun 22–24.
39. Barton, C.J., 1960. J. Phys. Chem. 64, 306–309.
40. Ward, W.T., Strehlow, R.A., Grimes, W.R., Watson, G.M., 1960. J. Chem. Eng. 5 (2), 137–142.
41. Atomic Energy Commission, 1971. Molten Salt Breeder Reactor Concept. Quarterly Report for the Period Ending July 21. NP-19145. Bombay: Atomic Energy Commission.
42. Capelli, E., Beneš, O., Konings, R.J.M., 2015. Thermodynamic assessment of the LiF–ThF_4–PuF_3 –UF_4 system. J. Nucl. Mater. 462, 43–53.
43. OSHA, 2018. Revising the Beryllium Standard for General Industry. Available at: https://www.federalregister.gov/documents/2018/12/11/2018-26448/revising-the-beryllium-standard-for-general-industry.
44. Koger, J.W., Litman, A.P., 1969. Compatibility of Hastelloy N and Croloy 9M With $NaBF_4$-NaF-KBF_4 (90-4-6 mol%) Fluoroborate Salt. ORNL-TM-2490.
45. Levin, E.M., Robbins, C.R., McMurdie, H.F., 1964. Phase Diagrams for Ceramists. Ohio: The American Ceramic Society, Inc.
46. Thoma, R.E., Sturm, B.J., 1965. Reactor Chemistry Division Annual Progress Report, ORNL-3789, p. 306, January 31, 1965.
47. Sooby, E.S., Nelson, A.T., White, J.T., McIntyre, P.M., 2015. Measurements of the liquidus surface and solidus transitions of the NaCl–UCl_3 and NaCl–UCl_3–$CeCl_3$ phase diagrams. J. Nucl. Mater. 466, 280–285.
48. Beneš, O., Konings, R.J.M., 2008. Thermodynamic evaluation of the NaCl–$MgCl_2$–UCl_3–$PuCl_3$ system. J. Nucl. Mater. 375 (2), 202–208.
49. Kraus, C.A., 1943. Phase Diagram of Some Complex Salts of Uranium With Halides of the Alkali and Alkaline Earth Metals. Report M-251.
50. Mourogov, A., Bokov, P.M., 2006. Potentialities of the fast spectrum molten salt reactor concept: REBUS-3700. Energy Convers. Manag. 47 (17), 2761–2771.
51. Till, C.E., Chang, Y.I., 2011. Plentiful Energy: The Story of the Integral Fast Reactor, the Complex History of a Simple Reactor Technoloogy, With Emphasis on Its Scientific Basis for Non-specialists. Charles E. Till and Yoon Il Chang.
52. Yamawaki, M., Koyama, T., 2016. Reducing the burden of high level radioactive waste with transmutation-proposal of integral molten salt fast reactor (IMSFR). J. Nucl. Radiochem. Sci. 16, 1–4.
53. MCFR, 2019. MCFR Solutions: Nuclear Innovation for New Options in American Industry (accessed 6.12.19) Available at: https://terrapower.com/technologies/mcfr.
54. Raiman, S.S., 2019. Compatibility Studies of Cladding Candidates and Advanced Low-Cr Superalloys in Molten NaCl-$MgCl_2$. ORNL/TM-20109/1132.
55. Petroski, R., Hejzlar, P., Todreas, N.E., 2009. Thermal hydraulic design of a liquid salt-cooled flexible conversion ratio fast reactor. Nucl. Eng. Des. 239 (12), 2612–2625.
56. Susskind, H., Hill, F.B., Green, L., *et al.*, 1960. Corrosion Studies for a Fused Salt-Liquid Metal Extraction Process for the Liquid Metal Fuel Reactor. BNL 585 Technical Report. Brookhaven National Laboratory.
57. Raiman, S.S., Lee, S., 2018. Aggregation and data analysis of corrosion studies in molten chloride and fluoride salts. J. Nucl. Mater. 511, 523–535.
58. Olander, D., 2002. Redox condition in molten fluoride salts, definition and control. J. Nucl. Mater. 300, 270–272.
59. DeVan, J.H., Evans, R.B.I., 1962. Corrosion Behavior of Reactor Materials in Fluoride Salt Mixtures. ORNL-TM-328.
60. Keiser, J.R., 1977. Status of Tellurium-Hastelloy N Studies in Molten Fluoride Salts. ORNL/TM-6002.
61. Manly, W.D., Adamson, G.M.J., Coobs, J.H., *et al.*, 1958. Aircraft Reactor Experiment-Metallurgical Aspects. ORNL-2349.
62. Weir, J.R., Douglas, D.A., Manly, W.D., 1957. Inconel as a Structural Material for a High-Temperature Fused-Salt Reactor. ORNL-2264.
63. Reiser, J.R., DeVan, J.H., Lawrence, E.J., 1979. Compatibility of molten salts with type 316 stainless steel and lithium. J. Nucl. Mater. 85–86, 295–298.
64. Guo, S., Shay, N., Wang, Y., Zhou, W., Zhang, J., 2017. Measurement of europium (III)/europium (II) couple in fluoride molten salt for redox control in a molten salt reactor concept. J. Nucl. Mater. 496, 197–206.
65. Briggs, R.B., 1965. Molten-Salt Reactor Program Semiannual Progress Report for Period Ending February 28, 1965. ORNL-3282.
66. Briggs, R.B., 1965. Molten-Salt Reactor Program Semiannual Progress Report for Period Ending February 28, 1965, ORNL-3812.
67. Briggs, R.B., 1964. ORNL-3708 Molten-Salt Reactor Program Semiannual Progress Report for Period Ending July 31, 1964.
68. Cherginets, V.L., Rebrova, T.P., Ponomarenko, T.V., Naumenko, V.A., Bryleva, E.Y., 2015. Study of the carbohalogenation process in molten KCl–NaCl equimolar mixture. React. Kinet. Mech. Catal. 116 (2), 327–337.
69. Cherginets, V.L., 2001. Handbook of Solvents. Canada: Chemical Technology Publishing, pp. 633–635. (Chapter 10.3).
70. Indacochea, J.E., Smith, J.L., Litko, K.R., Karell, E.J., Rarez, A.G., 2001. High-temperature oxidation and corrosion of structural materials in molten chlorides. Oxid. Metals 55 (1), 1–16.
71. Indacochea, J.E., Smith, J.L., Litko, K.R., Karell, E.J., 2011. Corrosion performance of ferrous and refractory metals in molten salts under reducing conditions. J. Mater. Res. 14 (5), 1990–1995.
72. Ambrosek, J., 2011. Molten Chloride Salts for Heat Transfer in Nuclear Systems. University of Wisconsin.
73. Shaffer, J.H., Strain, J.E., Cuneo, D.R., Kelly, M.J., 1960. Separation of Protactinium From Molten Salt Reactor Fuel Compositions. US3110555A.
74. Grimes, W.R., Shaffer, J.H., 1967. Recovery of Protactinium From Molten Fluoride Salts. US3395991A.
75. Uhlíř, J., 2007. Chemistry and Technology of Molten Salt Reactors – History and Perspectives. J. Nucl. Mater. 360 (1), 6–11.
76. Xue, H., 2015. Presentation: China's TMSR Programme. Oak Ridge National Laboratory.
77. Zou, C.Y., Cai, C.Z., Yu, C.G., Wu, J.H., Chen, J.G., 2018. Transition to thorium fuel cycle for TMSR. Nucl. Eng. Des. 330, 420–428.
78. Zou, C.Y., Cai, X.Z., Jiang, D.Z., *et al.*, 2015. Optimization of temperature coefficient and breeding ratio for a graphite-moderated molten salt reactor. Nucl. Eng. Des. 281, 114–120.
79. Wei, L., Shengwei, W., Jian, Y., *et al.*, 2012. Hydrogen Diffusion and Permeability Measuring Device. CN202471554U.
80. Hua, L., Wei, L., Shengwei, W., *et al.*, 2014. Gas-Liquid Separation Device, Use of Gas-Liquid Separation Device and Method for Separating Micro-Bubbles in Liquid Melt Salt. CN104771937A.
81. Was, G.S., 2016. Fundamentals of Radiation Materials Science: Metals and Alloys, second ed. Springer.
82. Koger, J.W., 1972. Alloy Compatibility With LiF–BeF_2 Salts Containing ThF_4 and UF_4. Tennessee: Oak Ridge National Lab., p. 49.
83. Keiser, J.R., 1977. Status of Tellurium – Hastelloy N Studies in Molten Fluoride Salts. ORNL.
84. Keiser, J.R., 1977. Compatibility Studies of Potential Molten-Salt Breeder Reactor Materials in Molten Fluoride Salts. ORNL-TM-5783. ORNL.
85. Koger, J.W., 1972. Mass Transfer Between Hastelloy N and a Molten Sodium Fluoroborate Mixture in a Thermal Convection Loop. ORNL Report TM-4721. Oak Ridge National Laboratory.
86. Koger, J.W., 1973. Evaluation of Hastelloy N Alloys After Nine Years Exposure to Both a Molten Fluoride Salt and Air at Temperatures From 700 to 560°C. ORNL-TM-4189. ORNL.
87. Koger, J.W., 1972. Effect of FeF_2 Addition on Mass Transfer in a Hastelloy N-LiF-BeF_2-UF_4 Thermal Convection Loop System. ORNL-TM-4188. ORNL.
88. Wang, M., Nai, Q., Qiu, J., *et al.*, 2018. Development of GH3535 Alloy for Thorium Molten Salt Reactor. Singapore: Springer, pp. 137–147.
89. Haubenreich, P.N., Engel, J.R., 1970. Experience with the molten-salt reactor experiment. Nucl. Appl. Technol. 8.
90. McCoy, H.E., 1978. Status of Materials Development for Molten Salt Reactors. Technical Report TM-5920. Oak Ridge National Laboratory.

91. Silverman, M.D., Huntley, W.R., Robertson, H.E., 1976. Heat Transfer Measurements in a Forced Convection Loop With two Molten-Fluoride Salts. ORNL/TM-5335. ORNL.
92. Bates, J.B., Young, J.P., Murray, M.M., Kohn, H.W., Boyd, G.E., 1972. Stability of BF_3OH^- ion in molten and solid $NaBF_4$ and $NaF \cdot NaBF_4$ eutectics. J. Inorg. Nucl. Chem. 34 (9), 2721–2727.
93. McCoy, H.E., Beatty, R.L., Cook, W.H., *et al.*, 1969. New developments in materials for molten-salt reactors. Nucl. Appl. Technol. 8.
94. Olson, L.C., Ambrosek, J.W., Sridharan, K., Anderson, M.H., Allen, T.R., 2009. Materials corrosion in molten LiF–NaF–KF salt. J. Fluor. Chem. 130 (1), 67–73.
95. DeVan, J.H., 1969. Effect of Alloying Additions on Corrosion Behavior of Nickel-Molybdenum Alloys in Fused Fluoride Mixtures. ORNL-TM-2021. ORNL.
96. Blood, C.M., 1964. Solubility and Stability of Structural Metal Difluorides in Molten Fluoride Mixtures. ORNL-TM-760. ORNL.
97. Wang, C., Chen, W., Chen, M., Chen, D., Yang, K., 2019. Corrosion behavior and elements interdiffusion between a Ni coating and GH3535 alloy with and without a CrN barrier in molten fluoride salts. J. Nucl. Mater. 514, 348–357.
98. Jiang, L., Fu, C.-T., Leng, B., *et al.*, 2019. Influence of grain size on tellurium corrosion behaviors of GH3535 alloy. Corros. Sci. 148, 110–122.
99. McNabb, M.C., 1976. Metallographic examination of samples exposed to tellurium containing environments. In Molten-Salt Reactor Program (ORNL-5132). ORNL. pp. 100–121. (Semiannual progress report for period ending February 29, 1976).
100. Arima, T., Takaki, M., Sato, I., *et al.*, 2003. Reaction of modified SUS316 with tellurium under low oxygen potentials. Corros. Sci. 45 (8), 1757–1766.
101. Blackstone, R., 1977. Radiation creep of graphite. An introduction. J. Nucl. Mater. 65, 72–78.
102. ASTM International, 2008. ASTM D7219-08. Standard Specification for Isotropic and Near-Isotropic Nuclear Graphites. West Conshohocken, PA: ASTM International.
103. MacPherson, H.G., 1959. Molten-Salt Reactor Project Quarterly Progress Report for Period Ending April 30, 1959. ORNL-2723. ORNL.
104. He, Z., Gao, L., Qi, W., *et al.*, 2015. Molten FLiNaK salt infiltration into degassed nuclear graphite under inert gas pressure. Carbon 84, 511–518.
105. Shen, K., Su, J., Zhou, H., *et al.*, 2015. Abrasion behavior of graphite pebble in lifting pipe of pebble-bed HTR. Nucl. Eng. Des. 293, 395–402.
106. Wu, B., Li, Y., Zhao, H.-S., *et al.*, 2018. Wear behavior of graphitic matrix of fuel elements used in pebble-bed high-temperature gas-cooled reactors against steel. Nucl. Eng. Des. 328, 353–358.
107. Tang, H., Qi, W., He, Z., *et al.*, 2017. Infiltration of graphite by molten 2LiF–BeF_2 salt. J. Mater. Sci. 52 (19), 11346–11359.
108. He, X., Song, J., Tan, J., *et al.*, 2014. SiC coating: An alternative for the protection of nuclear graphite from liquid fluoride salt. J. Nucl. Mater. 448 (1), 1–3.
109. He, X., Song, J., Xu, L., *et al.*, 2013. Protection of nuclear graphite toward liquid fluoride salt by isotropic pyrolytic carbon coating. J. Nucl. Mater. 442 (1–3), 306–308.
110. He, Z., Lian, P., Song, Y., *et al.*, 2018. Improving molten fluoride salt and Xe 135 barrier property of nuclear graphite by phenolic resin impregnation process. J. Nucl. Mater. 499, 79–87.
111. Song, J., Zhao, Y., Zhang, J., *et al.*, 2014. Preparation of binderless nanopore-isotropic graphite for inhibiting the liquid fluoride salt and Xe 135 penetration for molten salt nuclear reactor. Carbon 79, 36–45.
112. Song, J., Zhao, Y., He, X., *et al.*, 2015. Preparation of pyrolytic carbon coating on graphite for inhibiting liquid fluoride salt and Xe^{135} penetration for molten salt breeder reactor. J. Nucl. Mater. 456, 33–40.
113. He, X., Song, J., Tan, J., *et al.*, 2014. SiC coating: An alternative for the protection of nuclear graphite from liquid fluoride salt. J. Nucl. Mater. 448 (1–3), 1–3.
114. Zhang, W.-T., Zhang, B.-L., Song, J.-L., *et al.*, 2016. Microstructure and molten salt impregnation characteristics of a micro-fine grain graphite for use in molten salt reactors. New Carbon Mater. 31 (6), 585–593.
115. Cook, W.H., 1967. Molten-Salt Reactor Program Semiannual Progress Report for Period Ending August 31, 1967. ORNL/TM-4191. ORNL.
116. Engel, J.R., Steffy, R.C., 1971. Xenon Behavior in the Molten Salt Reactor Experiment. ORNL-TM-3464. ORNL.
117. Scott, D., Eatherly, W.P., 1969. Graphite and xenon behavior and their influence on molten-salt reactor design. Nucl. Appl. Technol. 8, 179–189.
118. He, Z., Lian, P., Song, Y., *et al.*, 2018. Protecting nuclear graphite from liquid fluoride salt and oxidation by SiC coating derived from polycarbosilane. J. Eur. Ceram. Soc. 38 (2), 453–462.
119. Olson, L.C., Fuentes, R.E., Martinez-Rodriguez, M.J., *et al.*, 2015. J. Sol. Energy Eng. 137, 1–8.
120. Zheng, G., Kelleher, B., Cao, G., *et al.*, 2015. Corrosion of 316 stainless steel in high temperature molten Li_2BeF_4 (FLiBe) salt. J. Nucl. Mater. 461, 143–150.
121. Zheng, G., He, L., Carpenter, D., Sridharan, K., 2016. Corrosion-induced microstructural developments in 316 stainless steel during exposure to molten Li_2BeF_4 (FLiBe) salt. J. Nucl. Mater. 482, 147–155.
122. Sellers, R.S., Cheng, W.-J., Kelleher, B.C., *et al.*, 2014. Corrosion of 316L stainless steel alloy and Hastelloy-N superalloy in molten eutectic LiF-NaF-KF salt and interaction with graphite. Nucl. Technol. 188 (192),
123. Snead, L.L., Burchell, T.D., Katoh, Y., 2008. Swelling of nuclear graphite and high quality carbon fiber composite under very high irradiation temperature. J. Nucl. Mater. 381 (1), 55–61.
124. Bonal, J.P., Wu, C.H., 1996. Neutron induced thermal properties changes in carbon fiber composites irradiated from 600 to 1000°C. J. Nucl. Mater. 230 (3), 271–279.
125. Katoh, Y., Snead, L.L., Henager, C.H., *et al.*, 2014. Current status and recent research achievements in SiC/SiC composites. J. Nucl. Mater. 455 (1), 387–397.
126. Koyanagi, T., Ozawa, K., Hinoki, T., Shimoda, K., Katoh, Y., 2014. Effects of neutron irradiation on mechanical properties of silicon carbide composites fabricated by nano-infiltration and transient eutectic-phase process. J. Nucl. Mater. 448 (1), 478–486.
127. Perez-Bergquist, A.G., Nozawa, T., Shih, C., *et al.*, 2015. High dose neutron irradiation of Hi-Nicalon Type S silicon carbide composites, Part 1: Microstructural evaluations. J. Nucl. Mater. 462, 443–449.
128. Katoh, Y., Snead, L.L., Szlufarska, I., Weber, W.J., 2012. Radiation effects in SiC for nuclear structural applications. Curr. Opin. Solid State Mater. Sci. 16, 143–152.
129. Katoh, Y., Snead, L.L., Henager Jr., C.H., *et al.*, 2014. Current status and recent research achievements in SiC/SiC composites. J. Nucl. Mater. 455, 297–387.
130. Katoh, Y., Ozawa, K., Shih, C., *et al.*, 2014. Continuous SiC fiber, CVI SiC matrix composites for nuclear applications: Properties and irradiation effects. J. Nucl. Mater. 448, 448–476.
131. Xue, W., Yang, X., Zhou, X., *et al.*, 2018. Effect of concentration of Cr^{3+} in LiF-NaF-KF salt on the corrosion of SiC. J. Nucl. Mater. 509, 527–531.
132. Yang, X., Liu, M., Gao, Y., *et al.*, 2016. Effect of oxygen on the corrosion of SiC in LiF–NaF–KF molten salt. Corros. Sci. 103, 165–172.
133. Xi, J., Jiang, H., Liu, C., Morgan, D., Szlufarska, I., 2019. Corrosion of Si, C, and SiC in molten salt. Corros. Sci. 146, 1–9.
134. Xue, W., Yang, X., Qiu, J., *et al.*, 2017. Effects of Cr^{3+} on the corrosion of SiC in LiF–NaF–KF molten salt. Corros. Sci. 114, 96–101.
135. Wang, H., Feng, Q., Wang, Z., *et al.*, 2017. The corrosion behavior of CVI SiC matrix in SiCf/SiC composites under molten fluoride salt environment. J. Nucl. Mater. 487, 43–49.
136. Wang, H., Feng, Q., Wang, Z., *et al.*, 2017. Microstructure evolution and high-temperature mechanical properties of SiCf/SiC composites in liquid fluoride salt environment. Corros. Sci. 124, 131–137.
137. Chan, K.J., Ambrecht, R.J., Luong, J.M., Choi, W.T., Singh, P.M., 2018. Carburization effects on the corrosion of Cr_Fe_Ni_W_ and Mo in Fluoride-scalt cooled high temperature reactor. Ann. Nucl. Energy 120, 279–285.
138. Guo, S., Zhang, J., Wu, W., Zhou, W., 2018. Corrosion in the molten fluoride and chloride salts and materials development for nuclear applications. Prog. Mater. Sci. 97, 448–487.
139. Yang, X., Zhang, D., Liu, M., *et al.*, 2016. Corrosion of SiC induced by Hastelloy N alloy and its corrosion products in LiF–NaF–KF molten salt. Corros. Sci. 109, 62–67.
140. Shrestha, S.L., Bhattacharyya, D., Yuan, G., *et al.*, 2016. Creep resistance and material degradation of a candidate Ni–Mo–Cr corrosion resistant alloy. Mater. Sci. Eng. A 674, 64–75.
141. Marsden, B.J., Haverty, M., Bodel, W., *et al.*, 2016. Dimensional change, irradiation creep and thermal/mechanical property changes in nuclear graphite. Int. Mater. Rev. 61 (3), 155–182.
142. American Society of Mechanical Engineer, 2015. ASME Boiler and Pressure Vessel Code, Sec. III, Div. 5 and Sec. VIII. New York: American Society of Mechanical Engineers, Boiler and Pressure Vessel Committee.